Journal of Medicinal Chemistry

Drug Annotation

Discovery of BIIB068: A Selective, Potent, Reversible Bruton's Tyrosine Kinase Inhibitor as an Orally Efficacious Agent for Autoimmune Diseases

Bin Ma, Tonika Bohnert, Kevin L Otipoby, Eric Tien, Million Arefayene, Judy Bai, Bekim Bajrami, Eris Bame, Timothy R Chan, Michael Humora, J Michael MacPhee, Douglas Marcotte, Devangi Mehta, Claire M Metrick, George A. Moniz, Evelyne Polack, Urjana Poreci, Annick Prefontaine, Sarah Sheikh, Patricia Schroeder, Karen Smirnakis, Lei Zhang, Fengmei Zheng, and Brian T Hopkins

J. Med. Chem., **Just Accepted Manuscript** • DOI: 10.1021/acs.jmedchem.0c00702 • Publication Date (Web): 22 Jul 2020

is published by the American Chemical Society. 1155 Sixteenth Street N.W., Washington, DC 20036

Discovery of BIIB068: a selective, potent, reversible Bruton's tyrosine kinase inhibitor as an orally efficacious agent for autoimmune diseases

Bin Ma [*], Tonika Bohnert, Kevin L. Otipoby [#], Eric Tien, Million Arefayene, Judy Bai, Bekim Bajrami, Eris Bame, Timothy R. Chan [§], Michael Humora [†], J. Michael MacPhee [¶], Douglas Marcotte [ƒ], Devangi Mehta [ɟ], Claire M. Metrick, George Moniz, Evelyne Polack, Urjana Poreci, Annick Prefontaine, Sarah Sheikh [ǂ], Patricia Schroeder [ƒ], Karen Smirnakis, Lei Zhang, Fengmei Zheng, Brian T. Hopkins [*].

Research & Development, Biogen, 225 Binney Street, Cambridge, MA, 02142, USA

ABSTRACT: Autoreactive B cell-derived antibodies form immune-complexes that likely play a pathogenic role in autoimmune diseases. In Systemic Lupus Erythematosus (SLE), these antibodies bind Fc receptors on myeloid cells and induce proinflammatory cytokine production by monocytes and NETosis by neutrophils. Bruton's tyrosine kinase (BTK) is a non-receptor tyrosine kinase that signals downstream of Fc receptors and plays a transduction role in antibody expression following B cell activation. Given the roles of BTK in both the production and sensing of autoreactive antibodies, inhibitors of BTK kinase activity may provide therapeutic value to patients suffering from autoantibody-driven immune disorders. Starting from an in-house proprietary screening hit followed by structure-based rational design, we have identified a

potent, reversible BTK inhibitor, BIIB068 (**1**), which demonstrated good kinome selectivity with good overall drug like properties for oral dosing, was well tolerated across preclinical species at pharmacologically relevant doses with good ADME properties, and achieved >90% inhibition of BTK phosphorylation (pBTK) in humans.

▪ INTRODUCTION

Bruton's Tyrosine Kinase (BTK) is a member of the Tec family of protein tyrosine kinases (TFK) that functions downstream of the B cell antigen receptor (BCR) in B cells and Fc receptors (FcRs) in myeloid cells such as neutrophils and basophils.[1] BTK activation drives the activation of key BCR-signaling pathways, phospholipase C-γ (PLCγ), phosphatidalyinositol-3-kinase/Akt and NF-κB, which eventually regulates B cell activation and expression of immunoglobulins (Ig). BTK plays a critical role in early B cell differentiation and mature B cell activation, and is expressed throughout B cell development but is lost upon terminal differentiation to plasma cells.[2] In 1952, Ogden Bruton[3] first reported a condition called X-linked agammaglobulinemia (XLA), manifested by lack of Igs and B cells,[4] that affects approximately 1 in 200,000 males.[5] Mutations in the X-linked BTK gene are responsible for the XLA phenotype.[6] Similarly, crippling mutations in the mouse BTK gene disrupt BTK expression and give rise to the X-linked immunodeficiency (xid) phenotype in mice, and those xid mice are resistant to acquiring lupus and collagen induced arthritis.[7] While BTK's role in B cell biology has been best characterized, inhibition of kinase activity with either covalent[8] or reversible BTK inhibitors[9] additionally exhibits functional effects in myeloid cell populations,[10] such as NETosis by neutrophils,[11] inflammation by basophils[12] and cytokine production by monocytes.[13]

For the past two decades, the pharmaceutical community has directed significant resources to identify BTK inhibitors[14] for potential therapeutic use in various oncology and auto-immune indications. Ibrutinib (**2**, Figure 1) is a first generation covalent BTK inhibitor that was approved by the FDA in 2013 to treat patients with mantle cell lymphoma (MCL) and chronic lymphocytic leukemia (CLL).[15] Acalabrutinib (**3**), a second generation, more selective covalent BTK inhibitor, exhibited a considerably improved safety profile (reduced adverse events of skin rash, and bleeding risk[16]) and was approved in 2017, followed in 2019 by the approval of Zanubrutinib (**4**),[17] another covalent BTK inhibitor from the same generation. Despite clinical success in oncology, some characteristics of these covalent inhibitors preclude them from use in autoimmune diseases that are often chronic. For example, elevations in liver aminotransferase levels were reported[18] with these covalent BTK inhibitors, both inherent and acquired resistance to drug activity has been reported in various lymphomas,[19] and an increased risk of idiosyncratic toxicity[20] is generally associated with covalent inhibitors. Therefore, the development of a reversible, selective BTK inhibitor may provide autoimmune patients a treatment with equivalent efficacy and a decreased risk profile.

Although numerous clinical trials have been reported targeting BTK inhibition as a potential treatment for autoimmune diseases (Spebrutinib[21] for rheumatoid arthritis (RA), Poseltinib[22] for RA and lupus, BMS-986195[23] for RA, Evobrutinib[24] for multiple sclerosis (MS), PRN1008[25] for pemphigus vulgaris, TAS5315 for RA[26], and Remibrutinib for chronic spontaneous urticaria and Sjogren's syndrome[27]), only three reversible BTK inhibitors[28] (Fenebrutinib, BMS-986142 and AS 1763) have been reported to be in clinic to date. The most advanced molecule is Fenebrutinib, which was recently reported by Roche/Genentech to have achieved the primary end point of ACR50 response in a phase II RA study[29], thus validating that inhibition of BTK

with a reversible small molecule can provide clinical efficacy for treatment of autoimmune indications such as RA when compared to covalent inhibitors.[30]

Here we report the identification of a highly selective reversible BTK inhibitor compound **1** (BIIB068) in phase I clinical trial for Lupus, from an in-house proprietary screening hit followed by structure-based rational design.

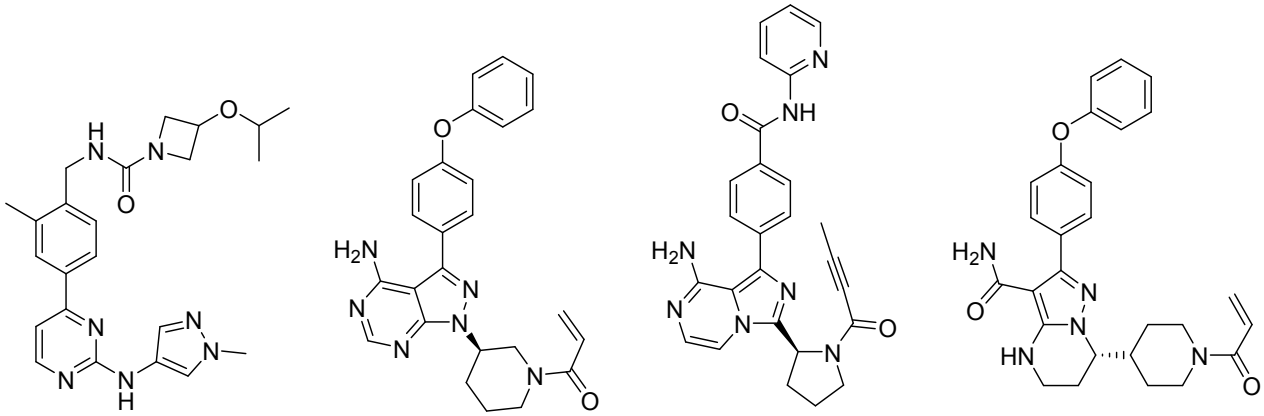

Figure 1. Chemical structures of BTK inhibitors BIIB068 (**1**), Ibrutinib (**2**), Acalabrutinib (**3**) and Zanubrutinib (**4**).

▪ RESULTS AND DISCUSSION

Hit optimization. The initial hit pyrrolopyrimidine **5** (BTK IC_{50} = 3700 nM, Figure 2) was identified from Biogen's internal proprietary screening collection.[31] It was co-crystalized with the BTK protein to obtain a structure to 1.4 Å resolution (Figure 3, Supplementary Table S-1). Compound **5** is an orthosteric ATP-competitive inhibitor which binds to the BTK in a DFG-in conformation. In contrast to Ibrutinib, which occupies the kinase back pocket behind the gatekeeper Tyr476 and interact with Cys481,[32] compound **5** binds to the hinge region within the

active site with the benzamide moiety reaching toward the pocket formed by Tyr551, Leu542 and Ser543 (termed as H3 pocket). Targeting the H3 pocket has been demonstrated to be essential for obtaining selectivity for BTK versus the other Tec family members.[33] Since this structure demonstrated ample room to grow into the H3 pocket toward Tyr551, the phenyl amide was augmented with a para *tert*-butyl group similar to CGI-1746.[33] This modification led to compound **6** (BTK IC_{50} = 142 ± 51 nM, N = 2), which exhibits more than 20-fold improvement in potency over compound **5**, though the ligand-lipophilicity efficiency (LLE = 1.8) remains low and comparable to that of compound **5** (LLE = 2.2). The kinase selectivity of compound **6** was profiled using the DiscoverX kinome panel and it showed modest selectivity (15/403 kinase > 80% inhibition @ 10 μM, Supplementary Table S-2), consistent with the *tert*-butyl group occupying the H3 pocket. An X-ray co-crystal structure of **6** was obtained to 1.6 Å resolution which confirmed this placement of the *tert*-butyl group (Figure 3, Supplementary Table S-1).

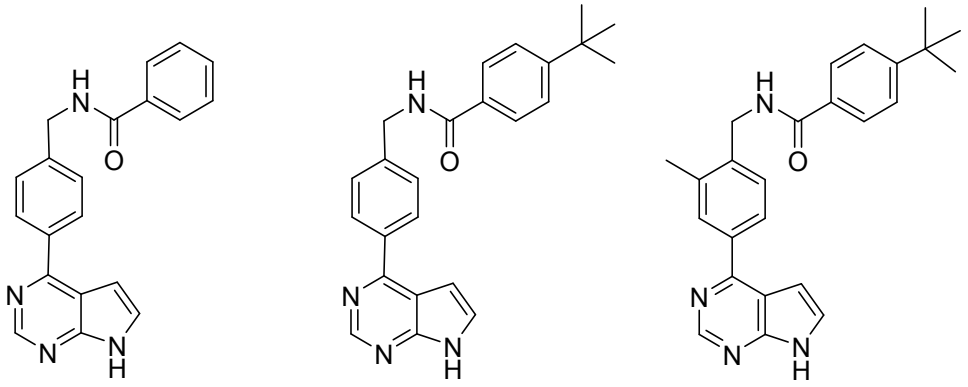

Figure 2. Chemical structures of novel pyrrolopyrimidine BTK hit **5** and analogs **6** and **7**.

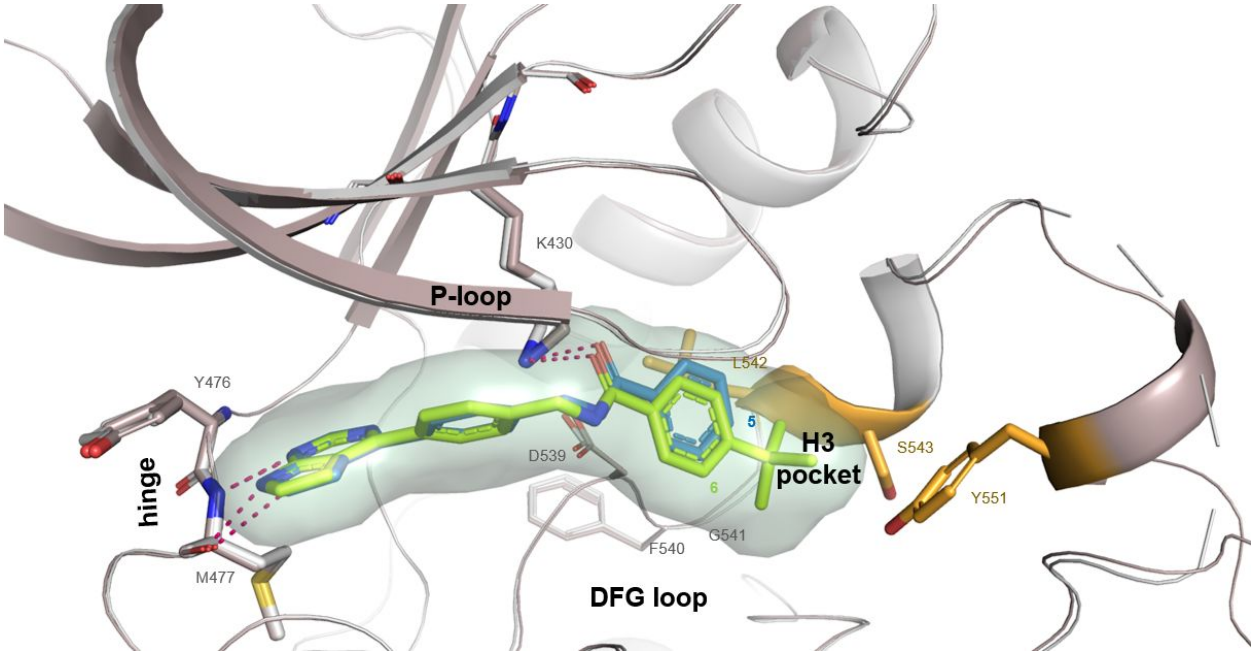

Figure 3. An overlay of BTK co-crystal structures with compound **5** (blue, PDB 6VXQ) and compound **6** (green, PDB 6W06) bound in the ATP active site. H3 residues Y551, S543 and L542 are marked in orange and structural features, binding interactions, and residues are labeled.

The co-crystal structure of **6** with BTK suggests that 2-substitution on the central phenyl core could reach towards the glycine rich P-loop and gain additional hydrophobic interactions (Supplementary Figure S-1). Thus, the next effort was focused on modifying the 2-position of the central phenyl ring to improve potency and LLE. As summarized in Table 1, adding a methyl group yielded compound **7** (BTK IC_{50} = 5 ± 0.1 nM, N = 2) with a 30-fold increase in potency and improved LLE (2.8 for **7** vs. 1.8 for **6**). Introducing larger hydrophobic substituents such as the ethyl or trifluoromethyl (**8** and **9**, BTK IC_{50} = 15 nM and 94 nM, respectively) was detrimental to the biochemical potency. Introducing polar moieties such as the primary amide in **10** (BTK IC_{50} = 3200 nM) led to a loss of activity. This is consistent with the in-silico docking

studies which suggested that small hydrophobic moieties were optimal for sitting in this pocket formed by lipophilic amino acid side chains.

Table 1. Characteristics of analogs of **6** featuring 2-substitution on the central phenyl core.

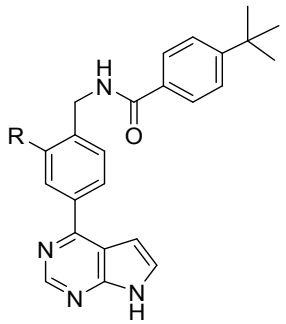

Compound	R	BTK IC_{50} (nM) [a]	Log D [b]	LLE
6	H	142	4.95	1.8
7	Me	5	5.18	2.8
8	Et	15	2.35	1.8
9	CF_3	94	2.43	1.1
10	$CONH_2$	3200	1.99	2.1

a IC_{50} values were determined using non-phosphorylated BTK protein in a FRET assay in duplicates.

b Measured using Analiza ELogD assay.

Compound **7** showed higher BTK potency and improved off target kinome selectivity (4/403 kinase > 80% @ 10 μM, FLT3, KIT, PDGFRB and YSK4, with K_d = 82, 150, 53 and 160 nM respectively) as compared to compound **6**. Despite the high lipophilicity with LogD = 5.18, compound **7** exhibited cellular activity (*in vitro* whole blood (WB) pBTK IC_{50} = 7.8 ± 0.2 μM, N

= 2). Thus, compound **7** was selected to advance to the next stage to optimize drug-like properties.

Hit to lead optimization. With the achievement of good biochemical potency and kinase selectivity by compound **7**, the next challenge for this series was to improve the poor drug-like properties represented by high LogD (5.18), poor aqueous solubility (kinetic solubility < 1 μg/ml at pH 6.8), weak WB cellular potency (IC_{50} = 7.8 μM), and high *in vivo* rat clearance (CL $\%Q_h$ > 90). To address these issues, our primary goals were to reduce the lipophilicity and improve the LLE of this chemical series. A series of compounds were synthesized in parallel to replace the distal 4-*tert*-butyl phenyl amide with various substituted 5- and 6-membered heteroaryl moieties. This effort led to the discovery of the isothiazole **11** which demonstrated comparable biochemical potency (BTK IC_{50} = 3 nM) and improved LLE (3.9) when compared to compound **7** (Table 2). Furthermore, compound **11** showed improved solubility (10 μg/mL at pH 6.8) and moderate *in vivo* clearance in rat IV PK (CL $\%Q_h$ = 43). Although an initial disconnect between *in vivo* and *in vitro* clearance rates (IVIVC) of compound **11** (*in vitro* RLM CL $\%Q_h$ > 90) was observed, correcting the *in vitro* clearance with plasma unbound fraction (fu) [34] (RLM CL $\%Q_h$ = 33), brought these values more in line. To investigate the contribution of the hinge binding moiety on the potency and ADME properties, the pyrrolopyrimidine hinge binder was replaced with either the 4-aminopyrimidine **12** or the 2-aminopyrimidine **13**. Both changes brought a modest improvement in the *in vitro* rat metabolic stability (RLM CL $\%Q_h$ = 72 and 65, respectively) and exhibited low clearance when dosed in the rat IV PK study (**12** CL $\%Q_h$ = 6 and **13** CL $\%Q_h$ = 11). The *in vivo* clearance values correlated with the fu-corrected *in vitro* rat clearance rates (**12** RLM CL $\%Q_h$ = 10 and **13** RLM CL $\%Q_h$ = 4).

Table 2. Characteristics of BTK inhibitors **11**, **12** and **13** featuring different hinge binders.

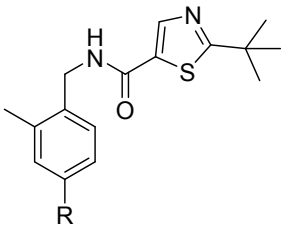

Compound	**11**	**12**	**13**
R	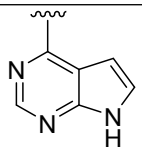	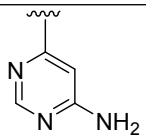	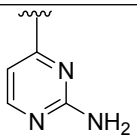
BTK IC_{50} (nM) [a]	3	9	6
LLE	3.9	4.1	4.4
Log D [a]	4.35	3.87	4.04
Solubility pH 6.8 (µg/mL) [b]	10	6	13
Human PPB fu % [c]	<1	3	<1
HLM/RLM (CL $\%Q_h$) [d]	64/91	53/72	56/65
Rat PK (CL $\%Q_h$) [e]	43	6	11

a See notes from Table 1.

b Measured using Analiza miniaturized shake flask.

c Unbound fraction was measured at a concentration of 2 µM for human plasma via rapid equilibrium dialysis (RED).

d Metabolic stability in human and rat liver microsome (%Qh hepatic blood flow (portal vein plus hepatic artery)).

e IV dosing in male SD rats, measured in triplicates.

Lead optimization to candidate. Having demonstrated the ability to attenuate the *in vivo* clearance while maintaining good biochemical potency and LLE, our efforts switched to further optimizing the biochemical potency and physicochemical properties of compound **13** in order to improve the WB cell activity (WB pBTK IC_{50} = 1.8 μM). The crystal structure of compound **6** (Supplementary Figure S-2) indicated that substituents adjacent to the hinge and extending toward the solvent front could interact with the surrounding residues (Leu408, Tyr476, Ala478 and Gly480) and potentially improve the biochemical potency. Introducing various alkyl substitutions on the amino group including Et, Me, *i*-Pr, *t*-Bu or cyclic alkyls decreased biochemical potency, but switching to aromatic substituents led to phenyl analog **14** which exhibited good biochemical potency (BTK IC_{50} = 1.8 nM) but did not show cellular activity likely due to the high lipophilicity (LogD = 3.44) and poor solubility (kinetic solubility < 1 μg/ml at pH 6.8) (Table 3). Introducing the 2-pyridine moiety **15** resulted in a loss in potency (BTK IC_{50} = 32 nM). Including the 4-pyridine compound **16** increased biochemical potency (BTK IC_{50} = 0.4 nM), however, like compound **14**, this improvement in biochemical potency was not paralleled by an improvement in the WB cell potency (WB pBTK IC_{50} = 5.3 μM). To further probe the SAR within this region of the protein, a series of 5-membered heteroaryl analogs were synthesized. Modulating the lipophilicity (LogD) by introducing substituted thiadiazole (**17**), isoxazole (**18**), and triazole (**19**) moieties resulted in compounds that were active in the biochemical assay. Unfortunately, even the most potent analog **18** (BTK IC_{50} = 1.7 nM) did not exhibit WB cellular activity. The most interesting SAR emerged with the synthesis of the 1,3 disubstituted pyrazole (**20**, BTK IC_{50} = 2.1 nM), which exhibited comparable activity in the WB cellular assay (WB pBTK IC_{50} = 4.7 μM) to pyridyl analog **16**, but with increased LogD (3.47). Appreciating the impact of the nitrogen atom within pyridyl-containing analogs

had on binding affinity, the 1,4-disubstituted pyrazole **21** was synthesized to mimic the placement of the pyridyl nitrogen. This adjustment provided a 10-fold improvement on both the biochemical potency and cellular activity (BTK IC_{50} = 0.2 ± 0.12 nM (N = 5), human WB pBTK IC_{50} = 0.43 ± 0.25 μM (N = 17)) and improved LLE (4.9) with higher LogD (4.76) (Table 3). Compound **21** exhibited low *in vivo* clearance and modest oral bioavailability (CL $\%Q_h$ = 6, IV 1 mg/kg, and %F = 24 in CMC/Tween) when dosed in rat. However, to further evaluate this chemical series in preclinical efficacy models, it was necessary to address the physicochemical properties including high LogD (4.76), low solubility (kinetic pH 6.8 <10 μg/mL) and high plasma protein binding (>99.5%).

Table 3. Characteristics of analogs of **13** featuring amino substitution off the pyrimidine hinge binder.

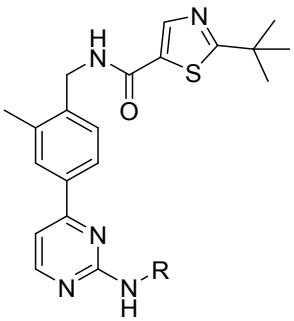

Compound	R	BTK IC_{50} (nM) [a]	Log D [a]	Solubility pH 6.8 μg/mL [a]	LLE
14	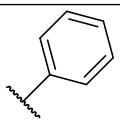	1.8	3.44	<0.1	2.2

15	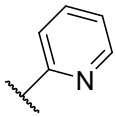	32	2.17	0.23	2.4
16	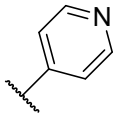	0.4	2.94	<0.1	4.2
17	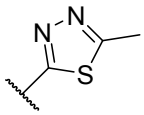	40	2.07	ND	2.8
18	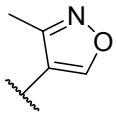	1.7	2.97	0.12	3.7
19	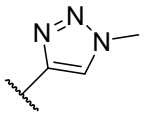	10	2.79	ND	4.1
20	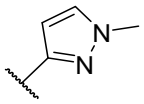	2.1	3.47	<0.1	4.0
21	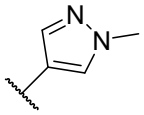	0. 2	4.76	2.7	4.9

a See notes from Table 2.

ND - not determined.

With the goal of reducing the lipophilicity of the lead series while maintaining the desirable biological and ADME properties of compound **21**, our attention moved to exploring the SAR around the amide moiety that occupies the H3 pocket. The thiadiazole analog **22** showed improved solubility but a notable loss in biochemical potency (0.2 nM vs 2 nM, Table 4), and a similar trend was observed with a few other types of heterocycles (data not shown). In-silico modelling studies suggested that sp^3 moieties such as 5-membered aliphatic groups would be

tolerated in place of the heteroaryl moiety, and that might improve the physicochemical properties of the series, including increasing solubility. To probe this hypothesis, the cyclopentyl analog **23** was synthesized. Compound **23** was less potent (BTK IC_{50} = 2 nM, tested as a mixture of 4 isomers) than **21** in the biochemical assay, however, its activity nevertheless validated the rationale that non-planar moieties might be tolerated in this position. Furthermore, the corresponding urea compound **24** showed significant improvement in both biochemical and cellular potency, as well as LLE (BTK IC_{50} = 0.2 nM, human WB pBTK IC_{50} = 0.35 μM, LLE = 5), though no improvement in solubility was observed. Additional attempts to enhance the solubility by reducing the lipophilicity led to the replacement of the pyrrolidine with the 3-substituted azetidine (**25**). This modification maintained good biological activity (BTK IC_{50} = 0.4 nM, human WB pBTK IC_{50} = 0.65 ± 0.79 μM (N = 3)) with lower LogD (3.34) but still no improvement in solubility was observed. Introducing an oxygen linkage at the 3-position of azetidine led to the discovery of compound **1** (BTK IC_{50} = 1 ± 1.1 nM, N = 5). This simple modification reduced lipophilicity (LogD = 2.32) substantially, improved the solubility, and reduced the plasma protein binding which all contributed to improving the WB cell potency (human WB pBTK IC_{50} = 0.12 ± 0.15 μM, N = 51).

Table 4. Characteristics of analogs of **21** featuring modifications to the distal H3 pocket region.

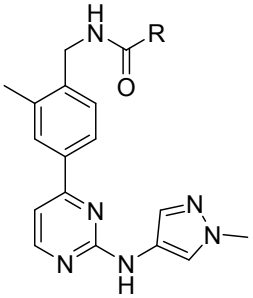

Compound	R	BTK IC_{50} (nM) [a]	LLE	Log D [a]	WB pBTK IC_{50} (μM) [b]	Unbound WB pBTK IC_{50} (nM) [c]	Human PPB fu% [a]	Corr. RLM, HLM CL %Q_h [a]	IV Rat % CL Q_h [a]	Solubility pH 1.5, 6.8 (μg/mL) [a]
21	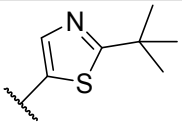	0. 2	4.9	4.76	0.43	1.3	0.3	1, 2	6	<10, <10
22	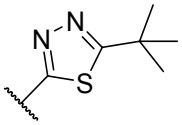	2	4.8	3.01	1.4	9.8	0.7	1, 3	18	>50, <10
23	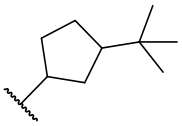	2	3.5	4.58	>10	7	0.07	3, 14	31	<10, <10
24	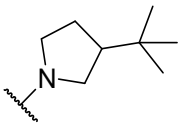	0. 2	5.0	3.72	0.35	0.7	0.2	1, 19	4	<10, <10
25	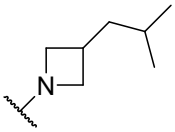	0.4	5.0	3.34	0.65	5.9	0.9	1, 8	17	<10, <10
1	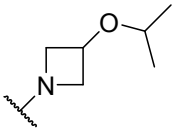	1	5.0	2.32	0.12	7.1	5.9	3, 9	1	>50, >10

a See notes from Table 2.

b Measured in duplicates except those stated in the text.

c Unbound WB pBTK IC_{50} = WB pBTK IC_{50} x Human PPB fu.

To sum up, focusing the medicinal chemistry strategy on optimizing the physicochemical properties of the lead series resulted in the discovery of compound **1**. Compound **1** exhibited improvement in *in vitro* biological potency, as well as good drug-like properties (LLE = 5) which resulted in low *in vivo* clearance (CL %Q_h = 6) and moderate oral bioavailability (%F = 48) when dosed in rats.

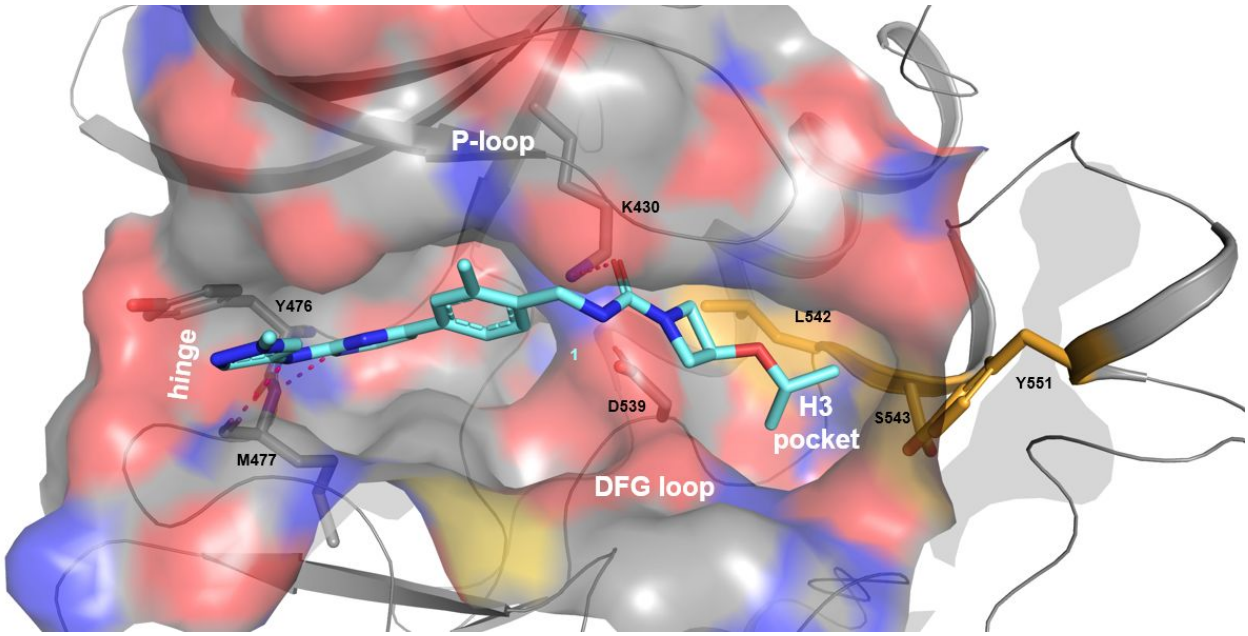

Figure 4. X-ray co-crystal structure of compound **1** in BTK (PDB 6W07). The active site surface is shown semi-transparent, and H3 residues Y551, S543 and L542 are marked in orange.

A co-crystal structure (Figure 4) of compound **1** bound in the active site of BTK confirmed that the 2-aminopyridimine moiety was acting as a dual hydrogen-bond acceptor/donor with residues in the hinge region of the protein. The methyl substituent on the phenyl core was positioned under the P-loop, and the benzyl urea linker oriented the azetidine into the H3 pocket which

sequestered Tyr551 in an inactive conformation. Similar to the published literature whereby binding in the H3 pocket of the active site conferred excellent kinome selectivity,[28a, 33] **1** hit only 10 kinases with >70% inhibition at 1 μM when screened against a panel of 395 kinases at DiscoverX (Supplementary Table S-3). Affinity measurement (K_d) were subsequently determined for all 10 kinases (Table 5),[35] which led to the conclusion that compound **1** yields > 400-fold selectivity for BTK versus all the other kinases tested including the structurally similar Tec family members (BMX, ITK, TEC, TXK).

Table 5. K_d values for kinases exhibiting > 70% affinity toward compound **1** relative to control at 1 μM.

Kinase name	**K_d (nM)**	**Selectivity fold over BTK**
Adaptor-associated protein Kinase 1 (AAK1)	430	1433
BMP2-Inducible Kinase (BMP2K)	1100	3666
BTK	0.3	-
Cyclin-dependent kinase-like 2 (CDKL2)	420	1400
Janus Kinase 2 (JAK2)	460	1533
Phosphatidylinositol-4-phosphare 5-Kinase type 1 Alpha (PIP5K1A)	>10000	>10000
RIO Kinase 1 (RIOK1)	1200	4000
RIO Kinase 2 (RIOK2)	2400	8000
Serine-threonine kinase (STK1)	880	2933
Mitogen-activated protein kinase kinase kinase 19 (YSK4)	130	433

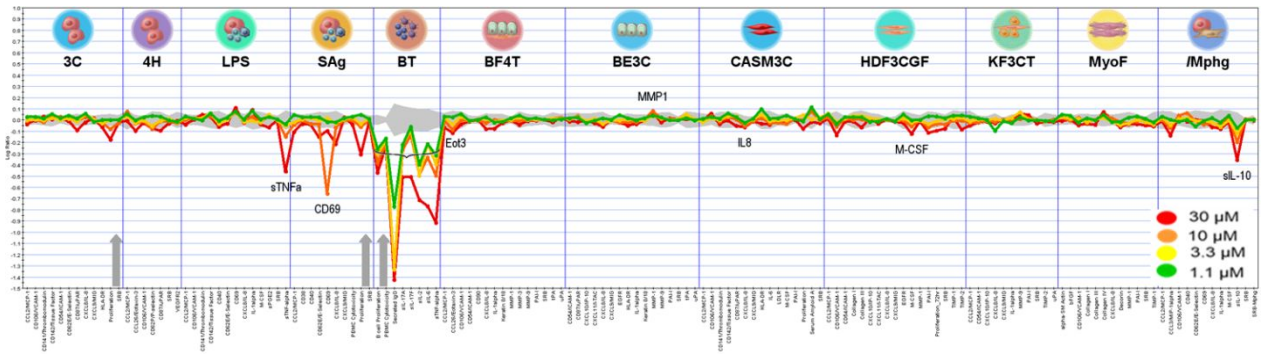

Figure 5. Phenotypic BioSeek study data of compound **1** at 1.1, 3.3, 10 and 30 µM. The gray area shows the 95% confidence area of each biomarker response in the absence of drug. Data points that fall outside of the gray area signify inhibition (below) or augmentation (above) of the biomarker response at the indicated concentration of compound **1**.

To further evaluate the selectivity of compound **1**, it was tested *in vitro* at 4 concentrations (30, 10, 3.3, and 1.1 µM) in the BioMAP system developed by BioSeek/DiscoverX. This platform comprises of 12 human primary cell-based assays that enable the assessment of both on- and off-target activity of a compound in a cellular system using pathway- and disease-relevant biomarkers.[36] Compound **1** exhibited dose-dependent activity which was restricted to the culture systems that included hematopoietic cells that express BTK protein (LPS, SAg, BT and Mphg). The predominant activity was observed in primary B cells and PBMCs (BT culture) and impacted biomarkers such as secreted IgG and sTNF-alpha (Figure 5). Furthermore, at 1.1 µM, the only culture system impacted by compound **1** was BT culture stimulated with anti-IgM and a sub-threshold amount of anti-TCR. Compared to the BioSeek literature data[37] of a nonselective BTK inhibitor Ibrutinib (Supplementary Table S-3) at the same concentration, which showed

activity in every cellular system, the BioSeek profile of compound **1** at 1.1 μM is consistent with its greater kinase selectivity.

In addition, compound **1** inhibited BCR mediated PLCγ2 phosphorylation in Ramos B cells (IC_{50} = 0.4 μM), anti-IgD induced and anti-IgM BCR-induced B cell activation in human PBMCs (IC_{50} = 0.11 μM and 0.21 μM, respectively) consistent with the activity on the BT culture system in the BioMAP study.

Drug metabolism & pharmacokinetics. Compound **1** exhibited low volume of distribution, low to moderate clearance in rat, dog and cynomolgus monkey, moderate oral bioavailability (26-32% in dogs and cynomolgus monkeys and 48% in rats), and a short half-life across species (Table 6). In *in vitro* ADME screening studies (Table 7), compound **1** exhibited high permeability and moderate efflux in the Caco-2 cell system. Tests for protein binding revealed a range across all preclinical species and humans, with fu_{rat} (1.28%) < fu_{cyno} (3.62%) < fu_{human} (5.95%) < fu_{dog} (11.3%). When evaluated for potential major human CYP-mediated drug-drug interactions, compound **1** did not inhibit any of the major CYP isoforms (1A2, 2C9, 2C19, 2D6, and 3A4) in human liver microsomes (IC_{50} > 25 μM) and did not result in CYP (1A2, 2B6, and 3A4) induction in the sandwich cultured human hepatocyte assay at concentrations up to 50 μM. Compound **1** was stable in the plasma of mouse, rat, beagle dog, cynomolgus monkey, and human (>95% parent compound remaining after 6 hours of incubation) and was not sequestered into the red blood cells of those species.

Compound **1** was extensively metabolized *in vitro* in liver microsomes and hepatocytes across all preclinical species (rat, dog, monkey) and humans. The primary biotransformation pathways of compound **1** in human liver microsomes were due to O-deisopropylation, oxidation at the

pyrazole moiety, and N-demethylation. Oxidation of the isopropyl group appeared to be a minor pathway, with additional minor metabolites formed by combinations of these primary pathways. Multiple CYPs were responsible for the oxidative metabolism with major (66%) contribution by 3A4 (K_I = 50 μM, k_{inact} = 0.08 h^{-1}). The metabolic pathways in liver microsomes and hepatocytes were similar across all four species with only quantitative differences detected. All metabolites detected in human liver microsomes and hepatocytes were also detected in more than one preclinical species, with no formation of unique human metabolites or any GSH or CN adducts. Overall, compound **1** showed acceptable ADME properties (Table 7) to warrant further development.

Table 6. Pharmacokinetics characteristics of compound **1** in preclinical species.

PK	**PO, 5 mpk** [a]			**IV, 1 mpk** [b]			
	AUC (ng*hr/mL)	**C_{max} (ng/mL)**	**%F**	**CL (mL/min/kg)**	**$t_{1/2}$ (h)**	**V_{ss}(L/kg)**	**%Q_h**
Rat	11907	2920	48	3	1.2	0.2	6
Dog	1938	652	26	11	2.1	1.2	37
Cyno	2346	282	32	11	0.9	0.7	26

a Vehicle: 0.1% CMC/ 0.2% Tween-80.

b Vehicle: 40% NMP solution for rat, and 70:30 PEG-400:H_2O solution for dog and cyno.

Table 7. Detailed *in vitro* profile of compound **1**.

Assay	**Result**
BTK IC_{50} (nM) [a]	1 ± 1.1 (N = 5)
BTK K_d (nM)	0.3 ± 0.2 (N = 2)
Human WB pBTK IC_{50} (μM) [a]	0.12 ± 0.15 (N = 51)
KINOMEscan @ 1 μM (>90% Control) [b]	1/394
	YSK4 (K_d = 130 nM)

Panlabs @ 10 μM (> 50% inhibition) [b]	2/68
	A_3(IC_{50} = 4.2 μM), H_2(IC_{50} = 26.5 μM)
CYP inhibition (1A2, 2C9, 2C19, 2D6, and 3A4) IC_{50} (μM) [b]	all isoforms >25
CYP 3A4 HLM time-dependent inhibition [b]	K_I = 50 μM, k_{inact} = 0.08 h^{-1}
LM (rat/dog/cyno/human) CL %Q_h [a]	2/8/26/7
hERG inhibition IC_{50} (μM) [c]	>50
HepG2 Cytotoxicity IC_{50} (μM) [b]	>20
Caco2 (P_{A-B}/Efflux ratio) [b]	15.4/4.1
PPB fu% (human) [a]	5.95
Aq. solubility (μg/mL, pH7/2) [d]	1/>100
Measured LogD7.4 (shake flask method)	2.92 ± 0.17 (N = 2)

a See notes from Table 4.

b. See supporting information.

c. In the automated patch-clamp assay.

d. In simulated intestinal fluid (pH7) and simulated gastric fluid (pH2).

Chemistry. Compound **1** was synthesized in seven steps starting with the commercially available 4-bromo-2-methylbenzonitrile **26** as shown in Scheme 1. Reduction of the nitrile moiety followed by Boc protection gave arylbromide **28**. To facilitate the aryl coupling to the pyrimidine moiety, it was necessary to first form the boronic ester **29**, followed by Suzuki coupling[38] to yield compound **30**. The 3-amino pyrazole moiety was installed via a palladium facilitated amination[39] and the Boc group was then removed upon treatment with HCl to produce the benzyl amine hydrochloride salt **32**. Finally, a CDI-mediated urea formation provided compound **1**. With a viable synthetic route in hand to support the synthesis for preclinical toxicology studies, it was deemed necessary to identify a crystalline form for further development. After an extensive salt screening, the hemi-adipate salt was identified as a suitable crystalline form with the necessary physicochemical properties for use in clinic.

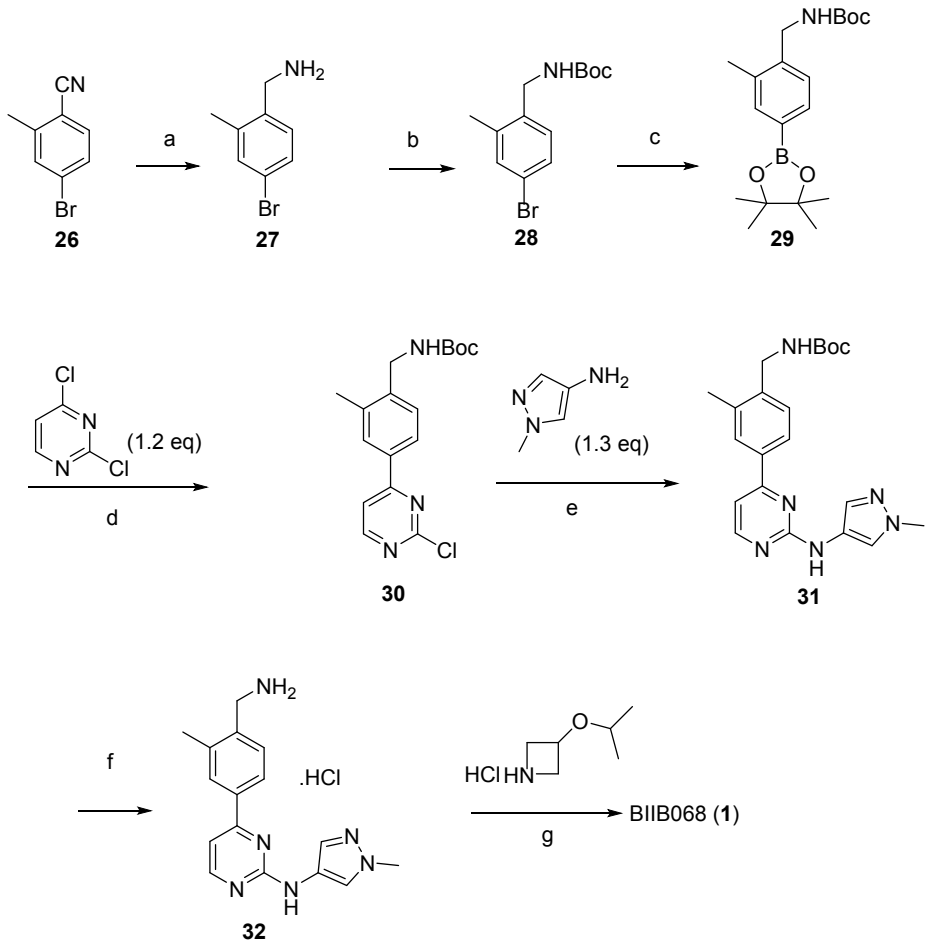

Scheme 1. Synthesis of BIIB068 (**1**). Reagents and conditions: (a) 3eq BH_3, THF, 0-80°C, 16hr, 90%; (b) 1.1 eq Boc_2O, 3 eq NEt_3, THF, rt, 1hr, 95%; (c) 1.2 eq PinB-BPin, 0.1 eq $Pd(dppf)Cl_2$, 3 eq KOAc, 1,4-dioxane, 100°C, 2hr, 69%; (d) 0.1 eq $Pd(dppf)Cl_2$, 2 eq K_2CO_3, 1,4-dioxane/H_2O (4:1), 90°C, 2hr, 80%; (e) 0.1 eq $Pd_2(dba)_3$, 0.2 eq S-Phos, 2 eq Cs_2CO_3, 1,4-dioxane, 120°C, 2hr, 63%; (f) HCl/MeOH, rt, 6hr, 90%; (g) CDI, DIPEA, DMF, 30%.

Efficacy and pharmacodynamic measures. BIIB068 (compound **1**) inhibits B cell, neutrophil and monocyte activation *in vitro*, but not T cell responses (Table 8). In an *in vitro* assay measuring total phosphorylated BTK (pBTK) in mouse WB, BIIB068 shows IC_{50} = 0.17 μM.

In further biological profiling, BIIB068 demonstrated dampening of BCR-mediated B cell activation, as measured by CD69 expression after PBMC simulation with anti-IgD (CD69 IC_{50} = 0.111 μM). After factoring protein binding, this value correlates well with the compound's ability to inhibit phosphorylation of BTK (IC_{50} = 1 nM) in the biochemical assay. Similarly, BIIB068 was shown to inhibit FcγR-mediated ROS production when added to human neutrophils from healthy donors that were activated with immune complexes (IC) from SLE patients (SLE IC) (IC_{50} = 0.054 μM). Blocking receptor access with antibodies to FcγRII (CD32) prevented SLE IC-mediated ROS production by neutrophils, demonstrating that the BIIB068 functional mechanism is dependent on FcγR signaling. Furthermore, to show that inhibition of BTK with BIIB068 selectively blocks B cell activation via BCR signaling, treatment of PBMCs with other receptor ligands including anti-CD40 and IL-4 in the presence of BIIB068 exhibited an IC_{50} = >10 μM for induction of CD69 expression on $CD19^+$ B cells. Collectively, the biological profile observed for BIIB068 was consistent with a molecule that selectively targets BTK.

Table 8. *In vitro* biological profile of BIIB068 (**1**).

Assay [a] (measured output, stimulus, cell type)	**IC_{50} ± SD (μM)**
B cell activation (CD69, anti-IgD/BCR, PBMC)	0.111 ± 0.087 (N = 10)
ROS generation (ROS, SLE IC/FcγR, neutrophils)	0.054 ± 0.057 (N = 4)
Monocyte (PB IgG, IL-6, IL-1b, TNFα/FcγR, PBMC)	0.063 ± 0.034 (N = 4)

pBTK inhibition (pTyr, n/a, human WB)	0.12 ± 0.15 (N = 51)
pBTK inhibition (pTyr, n/a, mouse WB)	0.17 ± 0.100 (N = 5)
B cell activation (CD69, IL-4/anti-CD40/CD40, PBMC)	>10
T cell activation (CD69, anti-CD3/CD28/TCR, PBMC)	>10

a See supporting information for assay conditions.

To understand the translatability from *in vitro* biological potency to *in vivo* efficacy, BIIB068 was tested in a thymus-independent type 2 (TI-2) antigen mouse model which had previously been reported to be BTK dependent.[40]

In contrast to thymus dependent (TD) antigens, thymus independent (TI) antigens induce a productive antibody response in neonatally thymectomized mice or nude mice, which also lack a thymus. TI antigens can be further differentiated based on whether they can (TI-1) or cannot (TI-2) generate an antibody response in xid mice. These three classes of model antigens differ in how they mechanistically induce an antibody response *in vivo*, with TI-2 antigens relying heavily on BCR signaling. BTK mutation was later shown to be the genetic cause responsible for the xid phenotype[41]. In retrospect, TI-2 antigens were defined as those antigens that require BTK expression to generate a productive antibody response *in vivo*, thus making it a well-suited *in vivo* efficacy model to test compounds that target BTK function.[42]

To directly evaluate the effects of BIIB068 on BTK-dependent B cell activation *in vivo*, the antigen-specific antibody response was measured from mice dosed orally with BIIB068 and immunized with a model TI-2 antigen (4-hydroxy-3-nitrophenyl) acetyl (NP) -Ficoll. Twice daily (BID) dosing of BIIB068 continued for 10 consecutive days. Serum, plasma, and WB were collected on day 10 to evaluate the antigen-specific antibody responses, plasma concentration of

BIIB068 and target engagement using the WB PD assay. NP-specific IgM antibody titers were compared to vehicle control animals. Substantial reductions of these antibody titers were observed in mice treated BID with 10-50 mg/kg/dose of BIIB068 (Figure 7). Specifically, anti-NP IgM antibody titers were reduced by 93%, 90%, 63%, 22% and -23% compared to vehicle control treated animals for BID BIIB068 doses of 50, 30, 10, 3 and 1 mg/kg/dose, respectively. The calculated ED_{50} of BIIB068 for IgM antibody titer was 4.4 mg/kg/dose. To further interrogate the pharmacokinetics of BIIB068 and degree of target engagement achieved in the TI-2 efficacy model, plasma and WB samples from each of the dose or vehicle arms were collected to determine exposures and degree of target engagement using pBTK assay concurrent with serum collection.

The pre-last dose group was used to determine the steady-state trough concentration of BIIB068 and the corresponding degree of target engagement in each dose arm. The samples taken at 1 and 4 hours after the final dose were used to determine the concentration and target engagement of BIIB068 at or near the t_{max} in each dose arm. The effects on the NP-specific antibody response are negligible during the maximum of 4-hour time difference between samples. Figure 6 shows the average inhibition of target engagement (% inhibition of pBTK figure 6B) or total exposure (nM, Figure 6C) in each dose group. BTK target engagement remains high, but dose-responsive, for at least 4 hours after PO dosing in all dose groups. In contrast, at steady-state trough levels of BIIB068 seen in the pre-last dose group, target-engagement is low or absent in all but in the highest dose arm, 50 mg/kg/dose. The duration of target engagement was dependent on the dose. The *in vivo* pBTK IC_{50} for BIIB068 is 0.13 μM (Supplementary Figure S-3), which is similar to the *in vitro* pBTK IC_{50} of 0.17 μM in mouse whole blood. The mice dosed with 30 mg/kg/dose show ~90% efficacy, indicating that full target coverage throughout the entire dosing period is

not necessary to drive high level of efficacy, at least in the TI-2 antibody response model. BIIB068 demonstrated good PK/PD correlation with *in vivo* EC_{50} = 0.16 μM based on antibody response, similar to *in vivo* WB pBTK potency in mice.

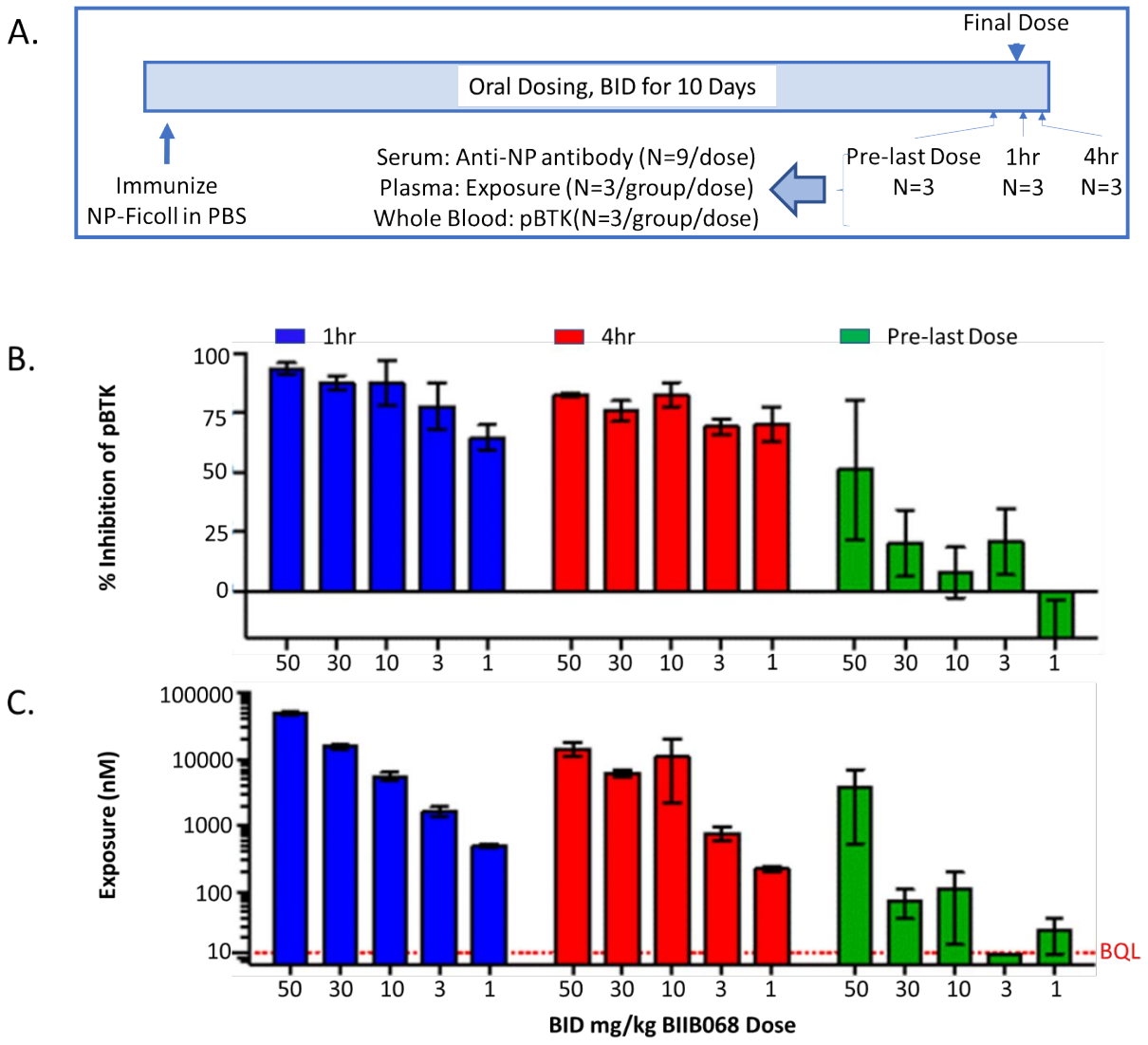

Figure 6. PK and PD analysis of BIIB068 (**1**) in the TI-2 efficacy model. A). workflow of the TI-2 mice efficacy model. B). pBTK % inhibition at 1 hr, 4 hr and pre-last dose. C). Total drug

concentration at 1 hr, 4 hr and pre-last dose. Figure shows mean and standard deviation of triplicate determination in one experiment.

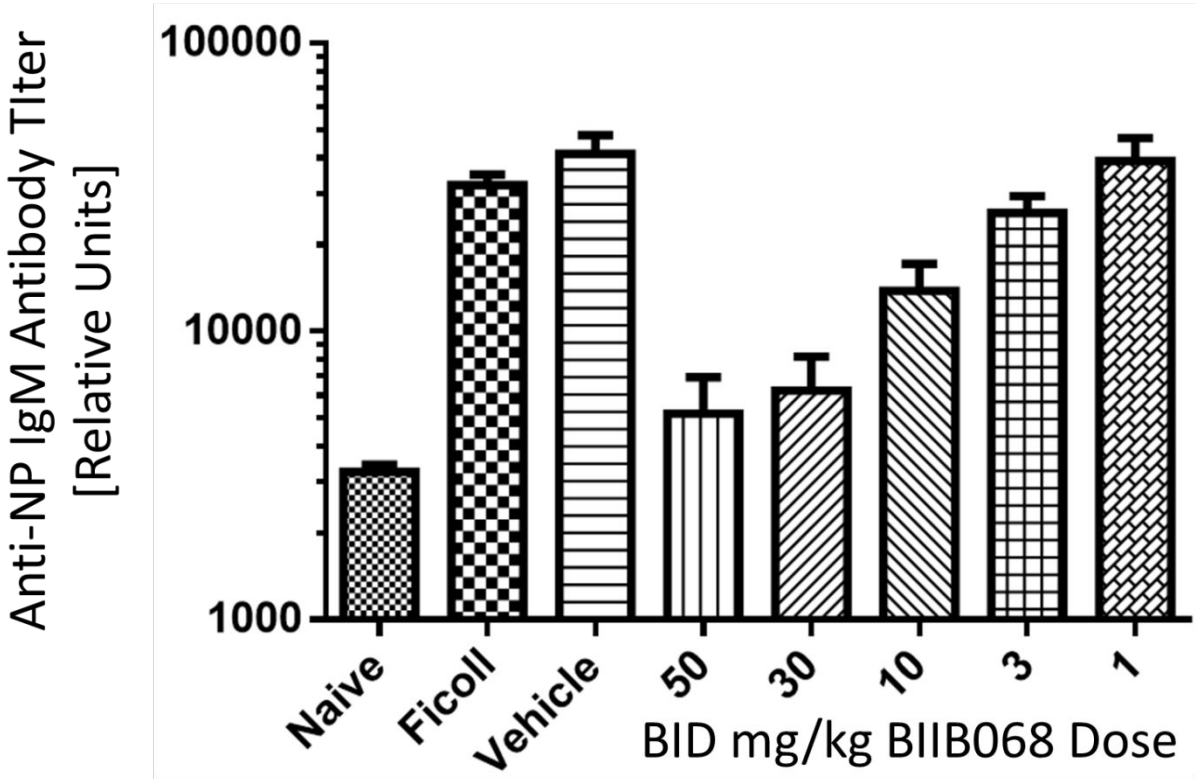

Figure 7. Dose response trial of BIIB068 (**1**)-mediated inhibition of the antigen-specific antibody response to a TI-2 antigen. Figure shows mean and standard deviation of triplicate determination in one experiment.

Preclinical safety. Toxicity profiling for BIIB068 was conducted in rodent (Sprague-Dawley rat) and non-rodent (cynomologus monkey) species for up to 13 weeks in GLP toxicity studies. The cynomologus monkey was chosen as the non-rodent species based on the similarities in metabolic profiles for BIIB068 in both human and monkey hepatocytes and microsomes. In both

the rat and monkey 13 weeks studies, BIIB068 was demonstrated to be safe and well tolerated. No compound related adverse effects in clinical signs, body weight, food consumption, ECG, clinical pathology, organ weight or gross pathology/histopathology were observed. BIIB068-related effects in rats were limited to non-adverse microscopic changes in the pancreas at ≥ 15 mg/kg/day.[43] Thus, the No Observed Adverse Effect Level (NOAEL) was determined at 50 mg/kg/day for rat and 100 mg/kg/day for monkey which corresponded to a daily rat AUC_{inf} 376 μg*hr/mL and monkey AUC_{inf} 129 μg*hr/mL.

BIIB068 exhibited no adverse effects in the single dose CNS and respiratory studies in rats nor in a single dose cardiovascular study in monkeys. BIIB068 demonstrates low genotoxic potential. BIIB068 was negative for clastogenic and mutagenic responses *in vitro* with and without metabolic activation (Aroclor-induced rat liver S9). BIIB068 was negative in the *in vivo* micronucleus assay in Sprague Dawley rats, where it showed no clastogenic activity and/or disruption of the mitotic apparatus in the bone marrow, and negative for micronuclei in rats.

Clinical study. Key human PK parameters were simulated utilizing both standard scaling IVIVE approaches extrapolated from the preclinical species' observed PK data and Simcyp® simulator (version 13) PBPK modeling. Clinical doses required to maintain a target level of EC_{75} for pBTK inhibition (based on TI-2 efficacy study)[44] in human WB for approximately > 10 hours coverage in a 12 hour dosing interval, was in the range of 50 mg/dose BID (100 mg/day) - 125 mg/dose BID (250 mg/day) daily dose. The phase I SAD study[45] was designed with goal of establishing the safety and tolerability for BIIB068. BIIB068 was dosed orally as a tablet in healthy volunteers at a starting dose of 10 mg which was chosen to afford > 10-fold margin to the NOAEL determined from the GLP preclinical toxicity studies**.** Dose escalation continued through the 120 mg cohort which based on the human PK had achieved exposures equivalent to

the NOAEL exposures (plasma total AUC) identified from the cyno GLP toxicity studies. BIIB068 was well tolerated with peak plasma concentration (C_{max}) occurring at ~0.9-2 hours after dosing and median $t_{1/2}$ ranges from 6-9 hours across all cohorts (Figure 8). BIIB068 was effective at inhibiting BTK phosphorylation and B-cell activation dose-dependently. At single doses ≥30 mg BIIB068, BTK phosphorylation was inhibited ≥70% for up to 12 hours post-dosing. Inhibition of BTK phosphorylation was ≥90% from approximately 1 hour through 8 hours post-dosing at 60 and 120 mg BIIB068. Peak inhibition occurred at approximately the same time as peak BIIB068 plasma concentration. Peak inhibition of B-cell activation (60%) occurred at 1 to 2 hours post-dosing (same time as peak BIIB068 plasma concentration) at 120 mg BIIB068 then gradually decreased by 8 hours post-dosing. Overall, BIIB068 was well tolerated and effective at inhibiting BTK phosphorylation in healthy subjects. BIIB068 also inhibited B-cell activation, although the inhibition was not as robust as inhibition of BTK phosphorylation. The reason why inhibition of B-cell activation was less robust than inhibition of BTK phosphorylation is unknown and may be a future area of investigation.[32] More details will be disclosed in due course.

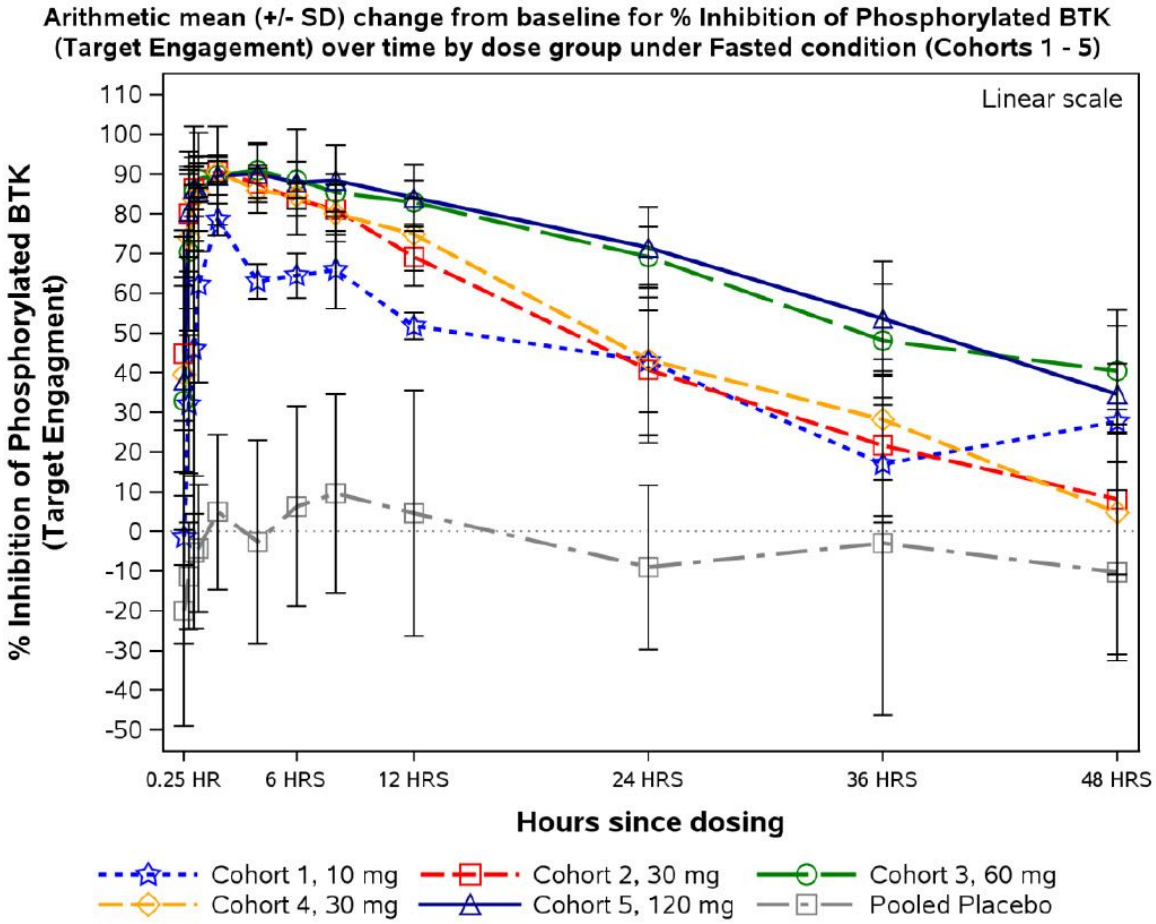
Arithmetic mean (+/- SD) change from baseline for % Inhibition of Phosphorylated BTK
(Target Engagement) over time by dose group under Fasted condition (Cohorts 1 - 5)
Linear scale
% Inhibition of Phosphorylated BTK
(Target Engagment)
110
100
90
80
70
60
50
40
30
20
10
0
-10
-20
-30
-40
-50
0.25 HR
6 HRS
12 HRS
24 HRS
36 HRS
48 HRS
Hours since dosing
Cohort 1, 10 mg
Cohort 2, 30 mg
Cohort 3, 60 mg
Cohort 4, 30 mg
Cohort 5, 120 mg
Pooled Placebo

A.

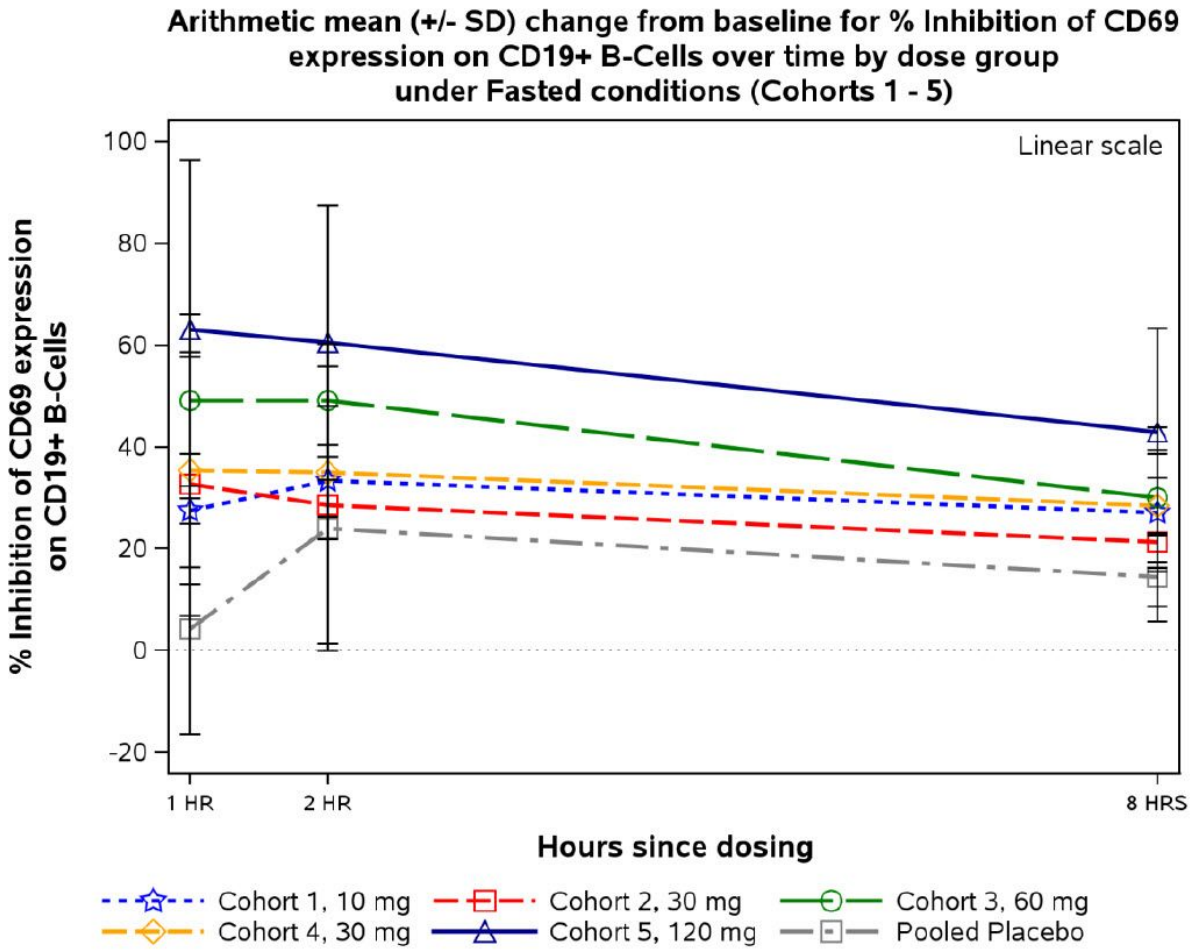
Arithmetic mean (+/- SD) change from baseline for % Inhibition of CD69 expression on CD19+ B-Cells over time by dose group under Fasted conditions (Cohorts 1 - 5)
Linear scale
% Inhibition of CD69 expression on CD19+ B-Cells
100
80
60
40
20
0
-20
1 HR
2 HR
8 HRS
Hours since dosing
Cohort 1, 10 mg
Cohort 2, 30 mg
Cohort 3, 60 mg
Cohort 4, 30 mg
Cohort 5, 120 mg
Pooled Placebo

B.

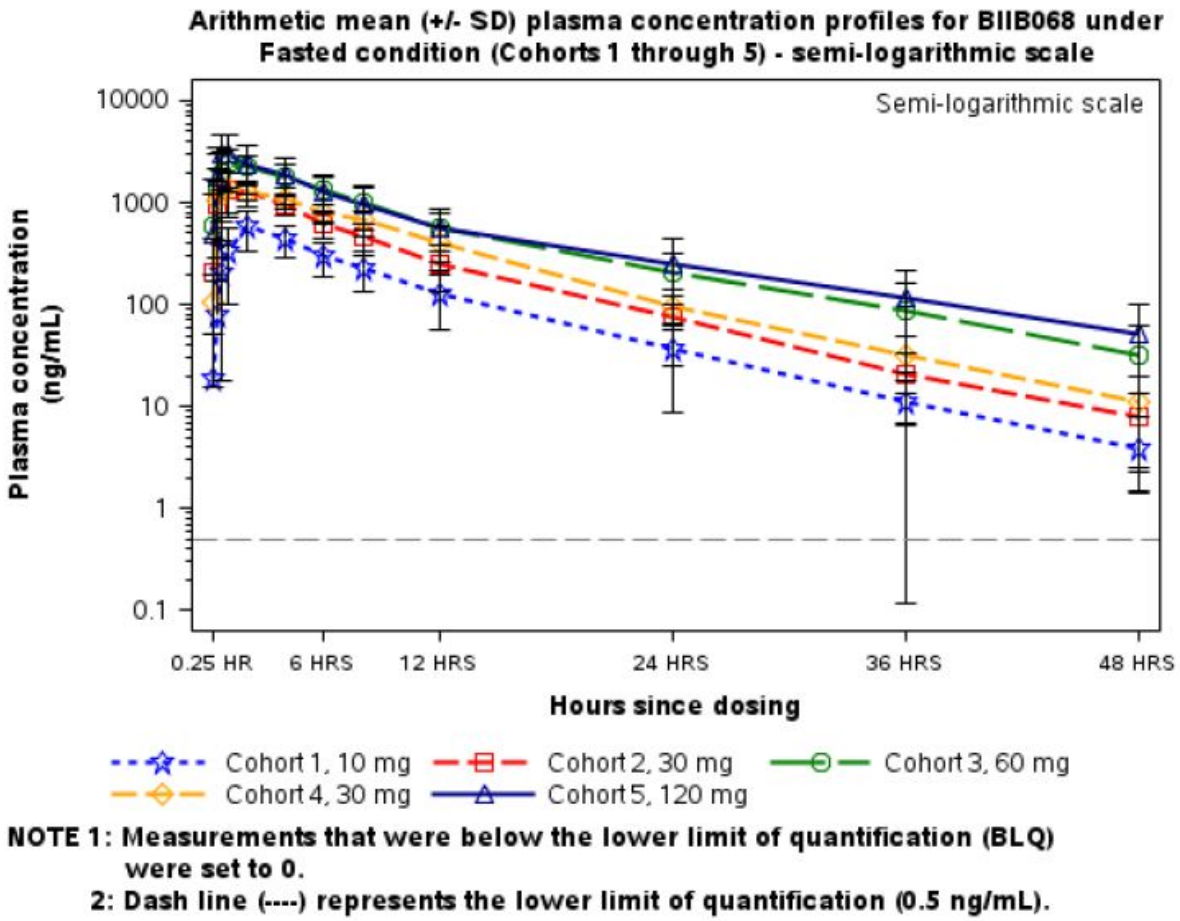

C.

Figure 8. Dose response of A). pBTK inhibition, B). CD69 expression inhibition by BIIB068, and C). Exposure of BIIB068 (**1**) in healthy human cohorts (Placebo, 10 mg, 30 mg, 60 mg, 120 mg).

▪ CONCLUSIONS

In summary, we have identified a selective, potent reversible BTK inhibitor BIIB068 through systematic rational drug design and optimization from a low micromolar screening hit. BIIB068 demonstrated favorable preclinical toxicology and DMPK properties across species which translated into good tolerability, PK, and target engagement in humans. The less robust inhibition of B cell activation measured by CD69 expression downstream of anti-IgD stimulation may

require additional studies to determine if this molecule has clinical significance as is or must be optimized further before use in clinic. Nevertheless, the discovery of BIIB068 represents a substantial progress of this series towards the successful use of a reversible BTK inhibitor for the treatment of autoimmune diseases.

▪ EXPERIMENTAL SECTION

General procedures. All solvents and chemicals were used as purchased from commercial sources without further purification. Reaction progress was monitored by LC-MS. Flash chromatography was performed with an Isco Combiflash Companion system using pre-packed silica gel columns. ^{1}HNMR and ^{13}CNMR spectra were recorded at 400 MHz using a Bruker Avance III spectrometer with a BBFO probe. Liquid chromatography was performed using a SunFire ™ C18, 3.5 μm, 4.6x20 mm IS ™ column with mobile phase of 0.1% TFA in H_2O (A) and 0.1% TFA in MeCN (B) and a gradient of 10-90% B with flow rate at 3.0 ml/min. Detector was set at dual wavelength 214 and 254 nm. The purity of all compounds listed was >95% at 254 nm.

(4-bromo-2-methylphenyl)methanamine (27). To a solution of 4-bromo-2-methylbenzonitrile (**26**) (3 g, 15 mmol) in THF (20 mL), BH_3·THF (45 mL, 45 mmol) was added. The solution was stirred at 0 °C for 1 hour and heated to 80 °C for 16 hours. Then the mixture was quenched with MeOH. After concentration, the residue was stirred with saturated HCl/EtOAc solution and filtered. The filter cake was rinsed with ether (20 mL x3) and dried under vacuum to afford titled product (3.2 g, yield 90%) as white solid. ESI-MS $(M+H)^+$: *m/z* 200.1. ^{1}H NMR (400 MHz, CD_3OD) δ: 7.25-7.51 (m, 3H), 4.15 (s, 2H), 2.41-2.44 (s, 3H).

tert-butyl 4-bromo-2-methylbenzylcarbamate (28). To a solution of (4-bromo-2-methylphenyl)methanamine (**27**) (1.2 g, 6 mmol) in DCM (30 mL), TEA (1.82 g, 18 mmol) and Boc_2O (1.43 g, 6.6 mmol) were added. The mixture was stirred at room temperature for 1 hour. After dilution with water (50 mL), the mixture was extracted with DCM (50 mL x2). The combined organics were washed with brine (50 mL), dried (Na_2SO_4), filtered and concentrated to give crude titled product (1.7 g, yield 95%) as a white solid, which was used directly in the next step without further purification. ESI-MS $(M+H)^+$: *m/z* 300.1. ^{1}H NMR (400 MHz, $CDCl_3$) δ: 7.28-7.33 (m, 2H), 7.11 (d, J = 8.03 Hz, 1H), 4.65-4.74 (m, 1H), 4.26 (br d, J = 5.77 Hz, 2H), 2.30 (s, 3H), 1.46 (s, 9H).

tert-butyl 2-methyl-4-(4,4,5,5-tetramethyl-1,3,2-dioxaborolan-2-yl)benzylcarbamate (29). To a solution of tert-butyl 4-bromo-2-methylbenzylcarbamate (**28**) (1.5 g, 5.0 mmol) in 1,4-dioxane (15 mL), 4,4,4',4',5,5,5',5'-octamethyl-2,2'-bi(1,3,2-dioxaborolane) (1.52 g, 6.0 mmol), KOAc (1.75 g, 18 mmol) and Pd(dppf)Cl_2.DCM (407 mg, 0.5 mmol) were added under N_2. The mixture was stirred at 100 ^oC for 2 hours. After cooling down to room temperature, the mixture was diluted with water (50 mL) and extracted with EtOAc (100 mL x3). The combined organic layer was washed with brine, dried, concentrated and purified by silica gel column (petroleum ether/EtOAc =10:1) to give titled product (1.2 g, yield 69%) as white solid. ESI-MS $(M+H)^+$: *m/z* 348.2. ^{1}H NMR (400 MHz, $CDCl_3$) δ: 7.61-7.59 (m, 2H), 7.26 (s, 1H), 4.68 (br, 1H), 4.33 (d, J = 5.6 Hz, 2H), 2.32 (s, 3H), 1.45 (s, 9H), 1.34 (s, 12H).

tert-butyl 4-(2-chloropyrimidin-4-yl)-2-methylbenzylcarbamate (30). To a solution of tert-butyl 2-methyl-4-(4,4,5,5-tetramethyl-1,3,2-dioxaborolan-2-yl)benzylcarbamate (**29**) (3.47 g, 10 mmol) and 2,4-dichloropyrimidine (1.79 g, 12 mmol) in 1,4-dioxane (28 mL) and H_2O (7 mL), Pd(dppf)Cl_2.DCM (815 mg, 1.0 mmol) and K_2CO_3 (2.76 g, 20 mmol) were added under N_2. The

mixture was stirred at 90 °C for 2 hours. After cooling to room temperature, the mixture was diluted with H_2O (80 mL) and extracted with EtOAc (80 mL x2). The organic layers were dried and concentrated. The residue was purified by column chromatography (silica, petroleum ether/EtOAc = 5:1 to 2:1) to give titled product (2.67 g, yield 80%) as white solid. ESI-MS $(M+H)^+$: *m/z* 334.1. ^{1}H NMR (400 MHz, $CDCl_3$) δ: 8.12 (d, J = 5.2 Hz, 1H), 7.92 (s, 1H), 7.87 (d, J = 8.0 Hz, 1H), 7.63 (d, J = 5.6 Hz, 1H), 7.40 (d, J = 7.6 Hz, 1H), 4.84 (br, 1H), 4.38(d, J = 5.2 Hz, 1H), 2.41 (s, 3H), 1.47 (s, 9H). ^{13}C NMR (101 MHz, $CDCl_3$) δ : 166.9, 161.8, 159.7, 155.7, 141.0, 136.9, 133.9, 129.2, 128.0, 125.1, 115.0, 79.8, 42.4, 28.3(3C), 19.0.

tert-butyl 2-methyl-4-(2-((1-methyl-1H-pyrazol-4-yl)amino)pyrimidin-4-yl)benzylcarbamate (31). To a solution of tert-butyl 4-(2-chloropyrimidin-4-yl)-2-methylbenzylcarbamate (**30**) **(**333 mg, 1.0 mmol) and 1-methyl-pyrazol-4-amine (126 mg, 1.3 mmol) in 1,4-dioxane (5 mL), $Pd_2(dba)_3$ (92 mg, 0.1 mmol), S-Phos (82 mg, 0.2 mmol) and Cs_2CO_3 (650 mg, 2.0 mmol) were added under N_2. The mixture was stirred at 120 °C for 2 hours. After cooling to room temperature, the mixture was diluted with H_2O (40 mL) and extracted with EtOAc (60 mL x2). The organic layers were dried and concentrated. The residue was purified by column chromatography (silica, petroleum ether/EtOAc = 3:1 to 1:1) to give titled product (248 mg, yield 63%) as white solid. ESI-MS $(M+H)^+$: *m/z* 395.1. ^{1}H NMR (400 MHz, CD_3OD) δ: 8.38 (d, J = 5.2 Hz, 1H), 7.97-7.93 (m, 3H), 7.65 (s, 1H), 7.38 (d, J = 8.0 Hz, 1H), 7.20 (d, J = 9.2 Hz, 1H), 4.30 (s, 2H), 3.85 (s, 3H), 2.42 (s, 3H), 1.48 (s, 9H).

4-(4-(aminomethyl)-3-methylphenyl)-N-(1-methyl-1H-pyrazol-4-yl)pyrimidin-2-amine (32). A mixture of tert-butyl 2-methyl-4-(2-((1-methyl-1H-pyrazol-4-yl)amino)pyrimidin-4-yl)benzylcarbamate (**31**) **(**3.94 g, 10.0 mmol) in a solution of HCl in methanol (30 mL, prepared from gas HCl) was stirred at room temperature for 6 hours. The solvent was removed and the

solid was rinsed with cold diethyl ether (100 mL). The solid was dried under vacuum to give titled product (2.97 g, yield 90%) as a yellow solid. ESI-MS $(M+H)^+$: *m/z* 295.1. ^{1}H NMR (400 MHz, D_2O) δ: 7.98-7.96 (m, 1H), 7.66-7.22 (m, 6H), 4.10 (s, 2H), 3.68 (s, 3H), 2.20 (s, 3H).

2-(tert-butyl)-N-(2-methyl-4-(2-((1-methyl-1H-pyrazol-4-yl)amino)pyrimidin-4-yl)benzyl)thiazole-5-carboxamide (21). To a mixture of 4-(4-(aminomethyl)-3-methylphenyl)-N-(1-methyl-1H-pyrazol-4-yl)pyrimidin-2-amine (**32**) (200 mg, 0.7 mmol), 2-(tert-butyl)thiazole-5-carboxylic acid (139 mg, 0.752 mmol), and N,N,N',N'-Tetramethyl-O-(7-azabenzotriazol-1-yl)uronium Hexafluorophosphate (0.32 g, 0.84 mmol) in DMF (1.58 mL, 20.4 mmol), N,N-Diisopropylethylamine (0.355 mL, 2.04 mmol) was added slowly and stirred at room temperature overnight. The mixture was filtered through Celite and washed with DMF and purified by prep HPLC to give titled product as a solid (217.5 mg, yield 70%). ESI-MS $(M+H)^+$: *m/z* 462.20. ^{1}H NMR (300 MHz, DMSO-d6) δ: 9.57 (s, 1H), 9.10 (t, J = 5.48 Hz, 1H), 8.46 (d, J = 5.29 Hz, 1H), 8.33 (s, 1H), 7.95 (m, 3H), 7.56 (s, 1H), 7.40 (d, J = 7.93 Hz, 1H), 7.28 (d, J = 5.29 Hz, 1H), 4.50 (d, J = 5.29 Hz, 2H), 3.65 (s, 3H), 2.42 (s, 3H), 1.39 (s, 9H). HRMS (ESI+): *m/z* calcd for $C_{24}H_{27}N_7OS$ $[M+H]^+$: 462.2071; Found: 462.2073.

3-isopropoxy-N-(2-methyl-4-(2-((1-methyl-1H-pyrazol-4-yl)amino)pyrimidin-4-yl)benzyl)azetidine-1-carboxamide (1). To a mixture of 4-(4-(aminomethyl)-3-methylphenyl)-N-(1-methyl-1H-pyrazol-4-yl)pyrimidin-2-amine hydrochloride (**32**) (200 mg, 0.7 mmol), 3-isopropoxy azetidine (113 mg, 0.747mmol), and N,N-carbonyldiimidazole (0.110 g, 0.679 mmol) in DMF (1.58 mL, 20.4 mmol), N,N-diisopropylethylamine (0.473 mL, 2.72 mmol) was added slowly and stirred at room temperature overnight. The mixture was filtered through Celite and washed with DMF and purified by prep HPLC to give titled product as a solid (82 mg, yield 30%). mp 179-181 ^oC. ESI-MS $(M+H)^+$: *m/z* 436.3. ^{1}H NMR (400 MHz, DMSO-d6) δ: 9.48 (s,

1H), 8.45 (d, *J* = 5.02 Hz, 1H), 7.91-7.95 (m, 3H), 7.55 (br. s., 1H), 7.35 (d, *J* = 8.53 Hz, 1H), 7.25 (d, *J* = 5.27 Hz, 1H), 6.84 (s, 1H), 4.15 - 4.48 (m, 3H), 3.90 - 4.13 (m, 2H), 3.83 (s, 3H), 3.46 - 3.69 (m, 3H), 2.36 (s, 3H), 1.08 (d, *J* = 6.27 Hz, 6H). ^{13}C NMR (101 MHz, DMSO-d6) δ: 164.3, 160.2, 160.1, 159.3, 141.8, 136.2, 135.6, 130.3, 128.7, 127.9, 124.7, 123.9, 120.8, 107.0, 70.7, 65.6, 57.9 (2C), 41.3, 39.2, 22.8 (2C), 19.3. HRMS (ESI+): *m/z* calcd for $C_{23}H_{29}N_7O_2$ $[M+H]^+$: 436.2456; Found: 436.2446.

Protein crystallography. Protein expression, purification, crystallography, and structure solution were performed as previously published[46] with additional refinement in Phenix.[47] In summary, a construct encoding the kinase domain of human BTK (residues 382-659) with a cleavable GST affinity tag was expressed via baculovirus infection in Sf9 insect cells. Crystallography-grade BTK was isolated from lysed cells by affinity purification on glutathione resin, removal of the GST tag, and size exclusion chromatography. Concentrated protein (5-6 mg/ml) was incubated with 0.5-1.0 mM compound and 0.1 M guanidine HCl before assembling sitting drop vapor diffusion trays in crystallization solution at pH 6.5 including ammonium sulfate or ammonium acetate and PEG5000 monomethyl ether (MME), PEG3350, or PEG2000 MME as precipitants. Crystals formed with or without seeding within 3-5 days at 4 °C, were cryoprotected in mother liquor containing additional PEG5000 MME and ethylene glycol or PEG200, and were flash frozen before data collection at the LRL-CAT beamline within the Advanced Photon Source (APS) or the PXI beamline at the Swiss Light Source (SLS). The structure was solved from processed data using molecular replacement and refined. Data collection and refinement statistics are listed in Supplementary Table S-1 and maps, models, and additional experimental details have been deposited to the RCSB Protein Data Bank (see Accession Codes below).

BTK biochemical activity assay. BTK activity and inhibitor efficacy was evaluated by monitoring the amount of phosphorylation of a fluorescein-labeled polyGAT peptide substrate (Invitrogen PV3611) in the presence of active BTK enzyme (Upstate 14-552), ATP, and compound. For a typical assay, 24 μL of a ATP/peptide master mix (final concentration; ATP 10 μM, polyGAT 100 nM) in kinase buffer (10 mM Tris-HCl pH 7.5, 10 mM $MgCl_2$, 200 μM Na_3PO_4, 5 mM DTT, 0.01% Triton X-100, and 0.2 mg/ml casein) was aliquoted into each well of a black 96-well plate (costar 3694) followed by 1 μL of a 4-fold, 40X compound titration in 100% DMSO and 15 uL of BTK enzyme mix in 1X kinase buffer (with a final concentration of 0.25 nM). After 30 minutes, the reaction was quenched with 28 μL 50 mM EDTA. 5 μL aliquots of the reaction mixture were transferred to a low volume, white 384-well plate (Corning 3674), and 5 μL of a 2X detection buffer (Invitrogen PV3574, with 4 nM Tb-PY20 antibody, Invitrogen PV3552) was added before a 45 minute incubation at room temperature in the dark and time resolved fluorescence (TRF) measurement on a Molecular Devices M5 (332 nm excitation; 488 nm emission; 518 nm fluorescein emission) instrument. IC_{50} values were calculated using a four-parameter fit with 100% enzyme activity determined from the DMSO control and 0% activity from the EDTA control.

pBTK WB assay. Heparinized venous WB was aliquoted into 96-well plate and "spiked" with serial dilutions of test compound in DMSO or with DMSO without drug. The final concentration of DMSO in all wells was 0.1%. The plate was incubated at 37°C for 30 min. Lysis buffer containing protease and phosphatase inhibitors was added to the drug-containing samples and one of the DMSO-only samples (+PPi, high control), while lysis buffer containing protease inhibitors was added to the other DMSO-only samples (-PPi, low control). All the lysed WB samples were subjected to the total BTK capture and phosphotyrosine detection method. ECL

values were graphed in Prism and a best-fit curve with restrictions on the maximum and minimum defined by the +PPi high and –PPi low controls was used to estimate the test compound concentration that results in 50% inhibition of ECL signal by interpolation.

Clinical pBTK assay. Heparinized venous WB was collected from patients enrolled in the study. Within 2 hours of collection, blood was aliquoted (200 μL) into appropriately labeled 1.2 mL cluster tubes. Samples were mixed with 200 μL of MSD Tris lysis buffer supplemented with protease and phosphatase inhibitors, followed by a 60 min incubation at 4 ^{o}C on a shaker set at a moderate speed. The lysed blood samples were stored at -70 ^{o}C until analyzed for phosphorylated and total BTK levels. MSD plates (anti-rabbit coated) were incubated overnight at 4 ^{o}C with rabbit anti-BTK antibody followed by treatment with blocking buffer. Frozen samples, standards, and appropriate QCs were thawed by soaking tubes in room temperature water for 5 mins and added to the MSD plates. BTK present in samples was captured on the plates during an overnight incubation at 4 ^{o}C. Subsequently, plates were incubated with either mouse anti-BTK antibody to detect total levels of the protein, or with anti-phosphorylated Tyrosine antibody to detect phosphorylated BTK. Phosphorylated BTK levels were normalized to total levels of BTK and the extent of inhibition was calculated based on pre-dose samples.

Clinical CD69 assay. Heparinized venous WB from patients enrolled in the clinical study were aliquoted (100 μL) into appropriately labeled 15 mL conical tubes. One set of aliquots received 0.1 μg/mL of anti-human IgD (clone IA6-2) conjugated to dextran. All samples were incubated at 37 ^{o}C/5% CO_2 for 18-24 hours. Upon incubation, samples were transferred to 12 x 75 mm FACS tubes and stained for 30 min at room temperature with a cocktail of antibodies containing anti-human CD19 (clone HIB19) conjugated to Allophycocyanin (APC) and anti-human CD69 (clone L78) conjugated to Phycoerythrin (PE). Red blood cells were lysed by incubating samples

for 10 min at room temperature with 2 mL of 1X FACSLyse solution. Upon lysis, remaining cells were washed with 2 mL of PBS supplemented with 1% Bovine Serum Albumin followed by fixation with 500 μL of 1% Paraformaldehyde solution. Samples were acquired on a properly calibrated BD flow cytometer and analyzed for CD69 expression on CD19+ gated B cells. Quantum™ R-PE MESF beads were utilized to standardize the fluorescence intensity of CD69. The extent of inhibition was calculated based on pre-dose samples.

TI-2 efficacy methods. Nine female DBA/1 mice (sourced from Charles River Discovery Research) per dose or vehicle arm were injected intraperitoneally with 30 μg of NP-Ficoll on day 0. BIIB068 was formulated in an aqueous vehicle of 0.5% Carboxymethylcellulose and 0.1% TWEEN 80 in water and dosed PO with BIIB068 twice a day for 10 days. The numbers on the x-axis in Figure 6B indicate the amount/dose administration that was given twice a day. Serum, WB, and plasma samples were collected on day 10 and stored at -80 ºC prior to assay. Serum was analyzed by ELISA for NP specific IgM. 96 well plates were pre-coated with NP-BSA, blocked and washed prior to adding serial diluted serum samples. Biotinylated anti-mouse IgM and streptavidin-HRP were sequentially used to detect NP-specific IgM antibodies. ABTS substrate was used to in a colorimetric assay to visualize the reaction, which was quantified by spectrophotometry at 405 nm. Softmax Pro Version 5.2 software was used to determine the levels of NP specific IgM antibodies present in the experimentally treated animals, relative to a standard curve of pooled NP-Ig positive serum. OD values from an eight-point dilution of each sample were used to interpolate relative antibody titer. Mean values for treatment groups were calculated and statistical significance was determined by one-way ANOVA followed by Dunnet's multiple comparison test. n = X/Normal Controls, n = 10/treatment group, *$p < 0.05$ ANOVA to Vehicle Control.

▪ ASSOCIATED CONTENT

Supporting Information.

The following file are available free of charge on the ACS Publications website at DOI:

Molecular formula strings (CSV).

Synthetic methods, characterization of key compounds, assay conditions, kinase selectivity data, receptor panel data, BioSeek data, and table of protein crystal data collection and refinement statistics. (PDF)

Accession Codes.

Structure data associated with this study have been deposited to the RCSB Protein Data Bank (http://www.rcsb.org) and can be accessed with the following codes: BTK bound to **1** is 6W07, to **5** is 6VXQ, and to **6** is 6W06. Authors will release the atomic coordinates and experimental data upon article publication.

▪ AUTHOR INFORMATION

Corresponding Authors

* Bin Ma. E-mail: bin.ma@biogen.com. Phone: 617-914-4955.

* Brian T. Hopkins. E-mail: brian.hopkins@biogen.com.

Present Addresses

Pandion Therapeutics, Cambridge, MA 02142.

† J-Star Research, South Plainfield, NJ 07080.

ƒ Forma Therapeutics, Watertown, MA 02472.

¶ Alkermes Inc., Waltham, MA 02451.

ɟ Immunologix Laboratories, Tampa, FL 33634.

§ Facebook, Redmond, WA 98052.

ǂ Takeda, Cambridge, MA 02142.

Author Contributions

All authors have given approval to the final version of the manuscript.

Funding Sources

Funding was provided by Biogen, who employed all authors at the time this research was conducted.

Notes

The authors declare no competing financial interest.

▪ ACKNOWLEDGEMENTS

The authors acknowledge Jiansheng Huang for collecting the HRMS data and the DMPK group for collecting all ADME data. Dr. Chuck Gu was greatly appreciated for helpful discussions on ADME properties. The authors thank Dr. Chris Helal for critical reviews. Adam Meyers was greatly appreciated for providing project management in multiple phases.

▪ ABBREVIATIONS

CDI, N,N-carbonyldiimidazole; ECG, Electrocardiogram; GLP, Good laboratory practice; IV, intravenous; IVIVC, In-Vivo In-Vitro Correlation; IVIVE, In-Vivo In-Vitro Extrapolation; HLM, human liver microsome; MS, Multiple Sclerosis; PBMC, peripheral blood mononuclear cell; PBPK, Physiologically based pharmacokinetic; RA, Rheumatoid arthritis; RLM, rat liver microsome; SAD, Single ascending dosing.

▪ REFERENCES

(1) (a) Young, R. M.; Staudt, L. M. Targeting pathological B cell receptor signaling in lymphoid malignancies. *Nat. Rev. Drug Discov.* **2013**, 12, 229-243. (b) Weber, A. N.; Bittner, Z.; Liu, X.; Dang, T.; Radsak, M. P.; Brunner, C. Bruton's tyrosine kinase: An emerging key player in innate immunity. *Front. Immunol.* **2017**, 8:1454. doi: 10.3389/fimmu.2017.01454.

(2) de Weers, M.; Verschuren, M. C.; Kraakman, M. E.; Mensink, R. G.; Schuurman, R. K.; van Dongen, J. J.; Hendriks, R. W. The Bruton's tyrosine kinase gene is expressed throughout B cell differentiation, from early precursor B cell stages preceding immunoglobulin gene rearrangement up to mature B cell stages. *Eur. J. Immunol.* **1993**, 23(12), 3109-3114.

(3) Bruton, O. C. Agammaglobulinemia. *Pediatrics.* **1952**, 9, 722-728.

(4) Smith, C. I. E.; Islam, K. B.; Vorechovsky, I.; Olerup, O.; Wallin, E.; Rabbani, H.; Baskin, B.; Hammarstrom, L. X-linked agammaglobulinemia and other immunoglobulin deficiencies. *Immunol. Rev.* **1994**, 138, 159-183.

(5) Chun, J.; Lee, T. J.; Song, J. W.; Linton, J. A.; Kim, D. S. Analysis of clinical presentations of Bruton disease: A review of 20 years of accumulated data from pediatric patients at severance hospital. *Yonsei Med. J.* **2008**, 49(1), 28–36.

(6) (a) Tsukada, S.; Saffran, D. C.; Rawlings, D. J.; Parolini, O.; Allen, R. C.; Klisak, I.; Sparkes, R. S.; Kubagawa, H.; Mohandas, T.; Quan, S.; Belmont, J. W.; Cooper, M. D.; Conley, M. E.; Witte, O. N. Deficient expression of a B cell cytoplasmic tyrosine kinase in human X-linked agammaglobulinemia. *Cell* **1993**, 72, 279–290. (b) Vetrie, D.; Vorechovski, I.; Sideras, P.; Holland, J.; Davies, A.; Flinter, F.; Hammarstrom, L.; Kinnon, C.; Levinsky, R.; Bobrow, M.; Smith, C. I.; Bentley, D. R. The gene involved in X-linked agammaglobulinemia is a member of the src family of protein tyrosine kinases. *Nature* **1993**, 361, 226–233.

(7) (a) Tsukada, S.; Rawlings, D. J.; Witte, O. N. Role of Bruton's tyrosine kinase in immunodeficiency. *Curr. Opin. Immunol.* **1994**, 6, 623-630. (b) Satoh, M.; Mizutani, A.; Behney, K. M.; Kuroda, Y.; Akaogi, J.; Yoshida, H.; Nacionales, D. C.; Hirakata, M.; Ono, N.; Reeves, W. H. X-linked immunodeficient mice spontaneously produce lupus-related anti-RNA helicase A autoantibodies but are resistant to pristane-induced lupus. *Int. Immunol.* **2003**, 5(9),1117-1124.

(8) Honigberg, L. A.; Smith, A. M.; Sirisawad, M.; Verner, E.; Loury, D.; Chang, B.; Li, S.; Pan, Z.; Thamm, D. H.; Miller, R. A.; Buggy, J. J. The Bruton tyrosine kinase inhibitor PCI-32765 blocks B cell activation and is efficacious in models of autoimmune disease and B cell malignancy. *Proc. Natl. Acad. Sci. U. S. A.* **2010**, 107, 13075−13080.

(9) Katewa, A.; Wang, Y.; Hackney, J. A.; Huang, T.; Suto, E.; Ramamoorthi, N.; Austin, C. D.; Bremer, M.; Chen, J. Z.; Crawford, J. J.; Currie, K. S.; Blomgren, P.; DeVoss, J.; DiPaolo, J. A.; Hau, J.; Johnson, A.; Lesch, J.; DeForge, L. E.; Lin, Z.; Liimatta, M.; Lubach, J. W.; McVay, S.; Modrusan, Z.; Nguyen, A.; Poon, C.; Wang, J.; Liu, L.; Lee, W. P.; Wong, H.; Young, W. B.; Townsend, M. J.; Reif, K. Btk-specific inhibition blocks pathogenic plasma cell signatures and

myeloid cell-associated damage in IFNα-driven lupus nephritis. *JCI Insight.* **2017**, 2, e90111. doi:10.1172/jci.insight.90111.

(10) Schmidt, U.; Boucheron, N.; Unger, B.; Ellmeier, W. The role of Tec family kinases in myeloid cells. *Int. Arch. Allergy Immunol.* **2004**, 134(1), 65-78.

(11) Florence, J. M.; Krupa, A.; Booshehri, L. M.; Davis, S. A.; Matthay, M. A.; Kurdowska, A. K. Inhibiting Bruton's tyrosine kinase rescues mice from lethal influenza-induced acute lung injury. *Am. J. Physiol. Lung Cell Mol. Physiol.* **2018**, 315(1), L52–L58.

(12) Smiljkovic, D.; Blatt, K.; Stefanzl, G.; Dorofeeva, Y.; Skrabs, C.; Focke-Tejkl, M.; Sperr, M. R.; Jaeger, U.; Valenta, R.; Valent, P. Bruton's tyrosine kinase inhibition is a potent approach to block IgE-mediated histamine release in human basophils. *Allergy.* **2017**, 72, 1666–1676.

(13) Ren, L.; Campbell, A.; Fang, H.; Gautam, S.; Elavazhagan, S.; Fatehchand, K.; Mehta, P.; Stiff, A.; Reader, B. F.; Mo, X.; Byrd, J. C.; Carson, W. E. III.; Butchar, J. P.; Tridandapani, S. Analysis of the effects of the Bruton's tyrosine kinase (Btk) inhibitor Ibrutinib on monocyte Fcγ receptor (FcγR) function. *J. Biol. Chem.* **2016**, 291(6), 3043-3052.

(14) (a) Akinleye, A.; Chen, Y. I.; Mukhi, N.; Song, Y.; Liu, D. Ibrutinib and novel BTK inhibitors in clinical development. *J. Hematol. Oncol.* **2013**, 6, 59. (b) Liang, C.; Tian, D.; Ren, X.; Ding, S.; Jia, M.; Xin, M.; Thareja, S. The development of Bruton's tyrosine kinase (BTK) inhibitors from 2012 to 2017: A mini-review. *Eur. J. Med. Chem.* **2018**, 151, 315-326. (c) Murphy, G.; Isenberg, D. A. New therapies for systemic lupus erythematosus - past imperfect, future tense. *Nat. Rev. Rheumatol.* **2019**, 15, 403-412. (d) Pal Singh, S.; Dammeijer, F.; Hendriks, R. W. Role of Bruton's tyrosine kinase in B cells and malignancies. *Mol. Cancer.* **2018**, 17(1), 57. doi:10.1186/s12943-018-0779-z.

(15) US Food and Drug Administration. Approved Drugs: Ibrutinib. Available at: https://wayback.archive-it.org/7993/20170111231706/http://www.fda.gov/Drugs/InformationOnDrugs/ApprovedDrugs/ucm374857.htm.

(16) Wu, J.; Zhang, M.; Liu, D. Acalabrutinib (ACP-196): a selective second-generation BTK inhibitor. *J. Hematol. Oncol.* **2016**, 9, 21. doi.org/10.1186/s13045-016-0250-9.

(17) (a) Guo, Y.; Liu, Y.; Hu, N.; Yu, D.; Zhou, C.; Shi, G.; Zhang, B.; Wei, M.; Liu, J.; Luo, L.; Tang, Z.; Song, H.; Guo, Y.; Liu, X.; Su, D.; Zhang, S.; Song, X.; Zhou, X.; Hong, Y.; Chen, S.; Cheng, Z.; Young, S.; Wei, Q.; Wang, H.; Wang, Q.; Lv, L.; Wang, F.; Xu, H.; Sun, H.; Xing, H.; Li, N.; Zhang, W.; Wang, Z.; Liu, G.; Sun, Z.; Zhou, D.; Li, W.; Liu, L.; Wang, L.; Wang, Z. Discovery of Zanubrutinib (BGB-3111), a novel, potent, and selective covalent inhibitor of Bruton's tyrosine kinase. *J. Med. Chem.* **2019**, 62(17), 7923-7940. (b) Wu, J.; Liu, C.; Tsui, S. T.; Liu, D. Second-generation inhibitors of Bruton tyrosine kinase. *J. Hematol. Oncol.* **2016**, 9:80. doi:10.1186/s13045-016-0313-y.

(18) Montalban, X.; Arnold, D. L.; Weber, M. S.; Staikov, I.; Piasecka-Stryczynska, K.; Willmer, J.; Martin, E. C.; Dangond, F.; Syed, S.; Wolinsky, J. S. Placebo-controlled trial of an oral BTK inhibitor in Multiple Sclerosis. *N. Engl. J. Med.* **2019**, 380(25), 2406-2417.

(19) Kaur, V.; Swami, A. Ibrutinib in CLL: a focus on adverse events, resistance, and novel approaches beyond ibrutinib. *Ann. Hematol.* **2017**, 96(7), 1175-1184.

(20) Ulrich, R. G. Idiosyncratic toxicity: A convergence of risk factors. *Annu. Rev. Med.* **2007**, 58, 17-34.

(21) Evans, E. K.; Tester, R.; Aslanian, S.; Karp, R.; Sheets, M.; Labenski, M. T.; Witowski, S. R.; Lounsbury, H.; Chaturvedi, P.; Mazdiyasni, H.; Zhu, Z.; Nacht, M.; Freed, M. I.; Petter, R.

C.; Dubrovskiy, A.; Singh, J.; Westlin, W. F. Inhibition of Btk with CC-292 provides early pharmacodynamic assessment of activity in mice and humans. *J. Pharmacol. Exp. Ther.* **2013**, 346, 219−228.

(22) A Study of LY3337641 in Rheumatoid Arthritis (RAjuvenate); ClinicalTrials.gov Identifier: NCT02628028, https://clinicaltrials.gov/ct2/show/NCT02628028.

(23) Watterson, S. H.; Liu, Q.; Beaudoin Bertrand, M.; Batt, D. G.; Li, L.; Pattoli, M. A.; Skala, S.; Cheng, L.; Obermeier, M. T.; Moore, R.; Yang, Z.; Vickery, R.; Elzinga, P. A.; Discenza, L.; D'Arienzo, C.; Gillooly, K. M.; Taylor, T. L.; Pulicicchio, C.; Zhang, Y.; Heimrich, E.; McIntyre, K. W.; Ruan, Q.; Westhouse, R. A.; Catlett, I. M.; Zheng, N.; Chaudhry, C.; Dai, J.; Galella, M. A.; Tebben, A. J.; Pokross, M.; Li, J.; Zhao, R.; Smith, D.; Rampulla, R.; Allentoff, A.; Wallace, M. A.; Mathur, A.; Salter-Cid, L.; Macor, J. E.; Carter, P. H.; Fura, A.; Burke, J. R.; Tino, J. Discovery of Branebrutinib (BMS-986195): a strategy for identifying a highly potent and selective covalent inhibitor providing rapid in vivo inactivation of Bruton's tyrosine kinase (BTK). *J. Med. Chem.* **2019**, 62(7), 3228-3250.

(24) Caldwell, R. D.; Qiu, H.; Askew, B. C.; Bender, A. T.; Brugger, N.; Camps, M.; Dhanabal, M.; Dutt, V.; Eichhorn, T.; Gardberg, A. S.; Goutopoulos, A.; Grenningloh, R.; Head, J.; Healey, B.; Hodous, B. L.; Huck, B. R.; Johnson, T. L.; Jones, C.; Jones, R. C.; Mochalkin, I.; Morandi, F.; Nguyen, N.; Meyring, M.; Potnick, J. R.; Santos, D. C.; Schmidt, R.; Sherer, B.; Shutes, A.; Urbahns, K.; Follis, A. V.; Wegener, A.A.; Zimmerli, S. C.; Liu-Bujalski, L. Discovery of Evobrutinib: an oral, potent, and highly selective, covalent Bruton's tyrosine kinase (BTK) inhibitor for the treatment of immunological diseases. *J. Med. Chem.* **2019**, 62(17), 7643-7655.

(25) Smith, P. F.; Krishnarajah, J.; Nunn, P. A.; Hill, R. J.; Karr, D.; Tam, D.; Masjedizadeh, M.; Funk, J. O.; Gourlay, S. G. A phase I trial of PRN1008, a novel reversible covalent inhibitor of Bruton's tyrosine kinase, in healthy volunteers. *Br. J. Clin. Pharmacol.* **2017**, 83(11), 2367-2376.

(26) Feng, Y.; Duan, W.; Cu, X.; Liang, C.; Xin, M. Bruton's tyrosine kinase (BTK) inhibitors in treating cancer: a patent review (2010-2018). *Expert Opin. Ther. Pat.* **2019**, 29(4), 217–241.

(27) Angst, D.; Gessier, F.; Janser, P.; Vulpetti, A.; Wälchli, R.; Beerli, C.; Littlewood-Evans, A.; Dawson, J.; Nuesslein-Hildesheim, B.; Wieczorek, G.; Gutmann, S.; Scheufler, C.; Hinniger, A.; Zimmerlin, A.; Funhoff, E. G.; Pulz, R.; Cenni, B. Discovery of LOU064 (remibrutinib), a potent and highly selective covalent inhibitor of Bruton's tyrosine kinase. *J. Med. Chem.* **2020**, 63, 5102−5118.

(28) (a) Crawford, J. J.; Johnson, A. R.; Misner, D. L.; Belmont, L. D.; Castanedo, G.; Choy, R.; Coraggio, M.; Dong, L.; Eigenbrot, C.; Erickson, R.; Ghilardi, N.; Hau, J.; Katewa, A.; Kohli, P. B.; Lee, W.; Lubach, J. W.; McKenzie, B. S.; Ortwine, D. F.; Schutt, L.; Tay, S.; Wei, B.; Reif, K.; Liu, L.; Wong, H.; Young, W. B. Discovery of GDC-0853: a potent, selective, and noncovalent Bruton's tyrosine kinase inhibitor in early clinical development. *J. Med. Chem.* **2018**, 61, 2227−2245. (b) Watterson, S. H.; De Lucca, G. V.; Shi, Q.; Langevine, C. M.; Liu, Q.; Batt, D. G.; Bertrand, M. B.; Gong, H.; Dai, J.; Yip, S.; Li, P.; Sun, D.; Wu, D.-R.; Wang, C.; Zhang, Y.; Traeger, S. C.; Pattoli, M. A.; Skala, S.; Cheng, L.; Obermeier, M. T.; Vickery, R.; Discenza, L. N.; D'Arienzo, C. J.; Zhang, Y.; Heimrich, E.; Gillooly, K. M.; Taylor, T. L.; Pulicicchio, C.; McIntyre, K. W.; Galella, M. A.; Tebben, A. J.; Muckelbauer, J. K.; Chang, C.; Rampulla, R.; Mathur, A.; Salter-Cid, L.; Barrish, J. C.; Carter, P. H.; Fura, A.; Burke, J. R.; Tino, J. A. Discovery of 6-Fluoro-5-(R)-(3-(S)-(8-fluoro-1-methyl-2,4-dioxo-1,2-dihydroquinazolin-3(4H)-yl)-2-methylphenyl)-2-(S)-(2-hydroxypropan-2-yl)-2,3,4,9-tetrahydro-

1H-carbazole-8-carboxamide (BMS-986142): a reversible inhibitor of Bruton's tyrosine kinase (BTK) conformationally constrained by two locked atropisomers. *J. Med. Chem.* **2016**, 59, 9173−9200. (c) Kawahata, W.; Asami, T.; Kiyoi, T.; Irie, T.; Taniguchi, H.; Asamitsu, Y.; Inoue, T.; Miyake, T.; Sawa, M. Design and synthesis of novel amino-triazine analogues as selective Bruton's tyrosine kinase inhibitors for treatment of Rheumatoid Arthritis. *J. Med. Chem.* **2018**, 61, 8917−8933.

(29) Cohen, S.; Tuckwell, K.; Katsumoto, T. R., Zhao, R.; Lee, C.; Berman, A.; Damjanov, N.; Fedkov, D.; Jeka, S.; Genovese, M. C. OP0025 Fenebrutinib compared to placebo and adalimumab in patients with inadequate response to either methotrexate therapy or prior TNF therapy: Phase 2 study. *Ann. Rheum. Dis.* **2019**, 78, 80-81.

(30) (a) Chan, P.; Yu, J.; Chinn, L.; Prohn, M.; Huisman, J.; Matzuka, B.; Hanley, W.; Tuckwell, K.; Quartino, A. Population pharmacokinetics, efficacy exposure-response analysis, and model-based meta-analysis of Fenebrutinib in subjects with Rheumatoid Arthritis. *Pharm. Res.* **2020**, 37:25. (b) Schafer, P.H.; Kivitz, A. J.; Ma, J.; Korish, S.; Sutherland, D.; Li, L.; Azaryan, A.; Kosek, J.; Adams, M.; Capone, L.; Hur, E. M.; Hough, D. R.; Ringheim, G. E. Spebrutinib (CC-292) affects markers of B cell activation, chemotaxis, and osteoclasts in patients with Rheumatoid Arthritis: Results from a mechanistic study. *Rheumatol. Ther.* **2020**, 7,101–119. (c) Genovese, M. C.; Spindler, A.; Sagawa, A.; Park, W.; Dudek, A.; Kivitz, A.; Chao, J.; Chan, L.; Barchuk, W.; Nirula, A. SAT0089 Safety and efficacy of LY3337641, a Bruton's tyrosine kinase inhibitor in patients with Rheumatoid Arthritis: A randomized, double-blinded, placebo-controlled, 2-part phase 2 study. *Ann. Rheum. Dis.* **2019**, 78, 1109-1110.

(31) Hopkins, B. T.; Bame, E.; Bell, N.; Bohnert, T.; Bowden-Verhoek, J. K.; Bui, M.; Cancilla, M. T.; Conlon, P.; Cullen, P.; Erlanson, D. A.; Fan, J.; Fuchs-Knotts, T.; Hansen, S.; Heumann,

S.; Jenkins, T. J.; Marcotte, D.; McDowell, B.; Mertsching, E.; Negrou, E.; Otipoby, K. L.; Poreci, U.; Romanowski, M. J.; Scott, D.; Silvian, L.; Yang, W.; Zhong, M. Optimization of novel reversible Bruton's tyrosine kinase inhibitors identified using tethering-fragment-based screens. *Bioorg. Med. Chem.* **2019**, 27, 2905–2913.

(32) Bender, A. T.; Gardberg, A.; Pereira, A.; Johnson, T.; Wu, Y.; Grenningloh, R.; Head, J.; Morandi, F.; Haselmayer, P.; Liu-Bujalski, L. Ability of Bruton's tyrosine kinase inhibitors to sequester Y551 and prevent phosphorylation determines potency for inhibition of Fc receptor but not B-cell receptor signaling. *Mol. Pharmacol.* **2017**, 91(3), 208-219.

(33) Di Paolo, J. A.; Huang, T.; Balazs, M.; Barbosa, J.; Barck, K. H.; Bravo, B. J.; Carano, R. A.; Darrow, J.; Davies, D. R.; DeForge, L. E.; Diehl, L.; Ferrando, R.; Gallion, S. L.; Giannetti, A. M.; Gribling, P.; Hurez, V.; Hymowitz, S. G.; Jones, R.; Kropf, J. E.; Lee, W. P.; Maciejewski, P. M.; Mitchell, S. A.; Rong, H.; Staker, B. L.; Whitney, J. A.; Yeh, S.; Young, W. B.; Yu, C.; Zhang, J.; Reif, K.; Currie, K. S. Specific Btk inhibition suppresses B cell- and myeloid cell-mediated arthritis. *Nat. Chem. Biol.* **2011**, 7, 41-50.

(34) (a) Obach, R. S. Nonspecific binding to microsomes: impact on scale-up of in vitro intrinsic clearance to hepatic clearance as assessed through examination of warfarin, imipramine, and propranolol. *Drug Metab. Dispos.* **1997**, 25(12), 1359-1369. (b) Choi, G.; Lee, Y.; Cho, H. Interpretation of non-clinical data for prediction of human pharmacokinetic parameters: in vitro-in vivo extrapolation and allometric scaling. *Pharmaceutics* **2019**, 11, 168.

(35) Copeland, R. A. *Evaluation of Enzyme Inhibitors in Drug Discovery;* John Wiley & Sons, Inc.: Hoboken, New Jersey, 2005; pp 141-177.

(36) Berg, E. L.; Yang, J.; Polokoff. M. A. Building predictive models for mechanism-of-action classification from phenotypic assay data sets. *J. Biomol. Screen.* **2013**, 18, 1260–1269.

(37) Haselmayer, P.; Camps, M.; Liu-Bujalski, L.; Nguyen, N.; Morandi, F.; Head, J.; O'Mahony, A.; Zimmerli, S. C.; Bruns, L.; Bender, A. T.; Schroeder, P.; Grenningloh, R. Efficacy and pharmacodynamic modeling of the BTK inhibitor Evobrutinib in autoimmune disease models. *J Immunol.* **2019**, 202(10), 2888-2906.

(38) Miyaura, N.; Suzuki, A. Palladium-catalyzed cross-coupling reactions of organoboron compounds. *Chem. Rev.* **1995**, 95 (7), 2457–2483. doi:10.1021/cr00039a007.

(39) Anderson, K.W.; Tundel, R.E.; Ikawa, T.; Altman, R.A.; Buchwald, S.L. Monodentate phosphines provide highly active catalysts for Pd-catalyzed CN bond-forming reactions of heteroaromatic halides/amines and (H)N-heterocycles. *Angew. Chem. Int. Ed. Engl.* **2006**, 45(39), 6523–6527. doi:10.1002/anie.200601612.

(40) (a) Khan, W. N.; Alt, F. W.; Gerstein, R. M.; Malynn, B. A.; Larsson, I.; Rathbun, G.; Davidson, L.; Muller, S.; Kantor, A. B.; Herzenberg, L. A.; Rosen, F. S.; Sideras, P. Defective B cell development and function in Btk-deficient mice. *Immunity*, **1995**, 3, 283-299. (b) Goess, C.; Harris, C. M.; Murdock, S.; McCarthy, R. W.; Sampson, E.; Twomey, R.; Mathieu, S.; Mario, R.; Perham, M.; Goedken, E. R.; Long. A. J. ABBV-105, a selective and irreversible inhibitor of Bruton's tyrosine kinase, is efficacious in multiple preclinical models of inflammation. *Mod. Rheumatol.* **2018**, 29, 510-522. doi:10.1080/14397595.2018.1484269.

(41) Drabek, D.; Raguz, S.; De Wit, T. P. M.; Dingjan, G. M.; Savelkoul, H. F. J.; Grosveld, F.; Hendriks, R. W. Correction of the X-linked immunodeficiency phenotype by transgenic expression of human Bruton tyrosine kinase under the control of the class II major histocompatibility complex Ea locus control region. *Proc. Natl. Acad. Sci. USA.* **1997**, 94(2), 610–615.

(42) Murphy, K. *Janeway's Immunobiology*; 8th ed. Garland Science: London, 2012; xix, 868 s.

(43) (a) Brenneman, K. A.; Ramaiah, S. K.; Rohde, C. M.; Messing, D. M.; O'Neil, S. P.; Gauthier, L. M.; Stewart, Z. S.; Mantena, S. R.; Shevlin, K. M.; Leonard, C. G.; Sokolowski, S. A.; Lin, H.; Carraher, D. C.; Jesson, M. I.; Tomlinson, L.; Zhan, Y.; Bobrowski, W. F.; Bailey, S. A.; Vogel, W. M.; Morris, D. L.; Whiteley, L. O.; Davis, J. W. II. Mechanistic investigations of test article–induced pancreatic toxicity at the endocrine–exocrine interface in the rat. *Toxicol. Pathol.* **2014**, 42, 229-242. (b) Xu, L.; Zhou, D.; Zhao, J.; Spolverato, G.; Zhang, Y.; Li, S.; Chen, M.; Pawlik, T. M. Long-term therapy with sorafenib is associated with pancreatic atrophy. *J. Surg. Res.* **2015**, 199(2), 314-321. (c) Erickson, R. I.; Schutt, L. K.; Tarrant, J. M.; McDowell, M.; Liu, L.; Johnson, A. R.; Lewin-Koh, S.-C.; Hedehus, M.; Ross, J.; Carano, R. A.; Staflin, K.; Zhong, F.; Crawford, J. J.; Zhong, S.; Reif, K.; Katewa, A.; Wong, H.; Young, W. B.; Dambach, D. M.; Misner, D. L. Bruton's tyrosine kinase small molecule inhibitors induce a distinct pancreatic toxicity in rats. *J. Pharmacol. Exp. Ther.* **2017**, 360, 226–238. (d) Bhaskaran, M.; Cornwell, P. D.; Sorden, S. D.; Elwell, M. R.; Russell, N. R.; Pritt, M. L.; Vahle, J. L. Pancreatic effects of a Bruton's tyrosine kinase small-molecule inhibitor in rats are strain-dependent. *Toxicol. Pathol.* **2018**, 46(4), 460-472. doi:10.1177/0192623318770163.

(44) Liu, L.; Di Paolo, J.; Barbosa, J.; Rong, H.; Reif, K.; Wong, H. Antiarthritis effect of a novel Bruton's tyrosine kinase (BTK) inhibitor in rat collagen-induced arthritis and mechanism-based pharmacokinetic/pharmacodynamic modeling: relationships between inhibition of BTK phosphorylation and efficacy. *J. Pharmacol. Exp. Ther.* **2011**, 338(1), 154-163.

(45) SLE: A Phase 1, Single-Ascending-Dose, Safety, Tolerability, Pharmacokinetic (PK), and Pharmacodynamic (PD) Study of BIIB068 in Healthy Participants; ClinicalTrials.gov Identifier: NCT02829541, https://clinicaltrials.gov/ct2/show/NCT02829541.

(46) Marcotte, D. J.; Liu, Y.-T.; Arduini, R. M.; Hession, C. A.; Miatkowski, K.; Wildes, C. P.; Cullen, P. F.; Hong, V.; Hopkins, B. T.; Mertsching, E.; Jenkins, T. J.; Romanowski, M. J,; Baker, D. P,; Silvian, L. F. Structures of human Bruton's tyrosine kinase in active and inactive conformations suggest a mechanism of activation for TEC family kinases. *Protein Sci.* **2010**, 19(3), 429-439.

(47) Adams , P. D.; Afonine, P. V.; Bunkóczi, G.; Chen, V. B.; Davis, I. W.; Echols, N.; Headd, J. J.; Hung, L.; Kapral, G. J.; Grosse-Kunstleve, R. W.; McCoy, A. J.; Moriarty, N. W.; Oeffner, R.; Read, R. J.; Richardson, D. C.; Richardson, J. S.; Terwilliger, T. C.; Zwart, P. H. PHENIX: a comprehensive Python-based system for macromolecular structure solution. *Acta Crystallogr. D. Biol. Crystallogr.* **2010**, 66, 213–221.

Table of Contents graphic

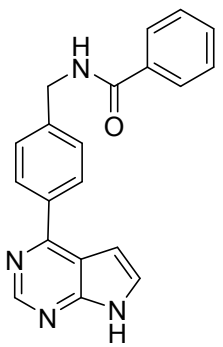

Hit
BTK IC_{50} = 3.7 μM
LLE 2.2

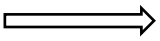

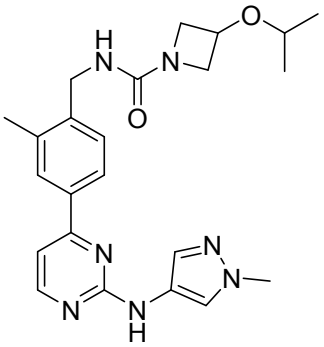

BIIB068 (1)
BTK IC_{50} = 1 nM
Human WB IC_{50} = 0.12 μM
LLE 5.0